Engineering Geology 280 (2021) 105954

Contents lists available at ScienceDirect

Engineering Geology

journal homepage: www.elsevier.com/locate/enggeo

Screening-level analyses for the evaluation of the seismic performance of a zoned earth dam

Giovanni Biondi [a], Ernesto Cascone [a,*], Domenico Aliberti [a], Sebastiano Rampello [b]

[a] Department of Engineering, University of Messina, Contrada di Dio, S. Agata, 98166 Messina, Italy
[b] Department of Structural and Geotechnical Engineering (DISG), Sapienza University of Rome, via Eudossiana 18, 00184 Rome, Italy

ARTICLE INFO

Keywords:
Zoned earth dam
Input motion selection
Displacement analyses
Shear strength reduction

ABSTRACT

Many existing earth dams have been designed and built worldwide before the establishment of a seismic code, so that it is of relevant interest to evaluate their seismic performance and post-seismic operational conditions. This requires an accurate geotechnical characterisation of the dam and foundation soils, a proper definition of the seismic scenarios at the site of the dam, the use of simplified procedures for screening-level seismic analyses and advanced non-linear dynamic analyses to study the most critical seismic scenarios.

This process has been used for the evaluation of the seismic performance of a zoned earth dam located in a high seismic hazard area of Southern Italy.

In this paper the available data of historical seismicity at the site of the dam and the results of a probabilistic seismic hazard analysis are first discussed and input ground motions are selected using compatibility criteria with the energy and frequency content of the expected target motion in a range of vibration period relevant for the non-linear response of the dam. Seismic performance of the dam is then evaluated through procedures based on Newmark-type computations, in which permanent displacements are related to ground motion characteristics and to the seismic resistance of the dam, the latter evaluated detecting the earthquake-induced plastic mechanisms and the corresponding critical accelerations. Also, an original improvement of the well-known Makdisi & Seed procedure, was proposed to better capture the actual influence of non-linear soil behaviour in the evaluation of horizontal acceleration and permanent displacements of the crest of the dam. The analysis results pointed out the relevant role of the earthquake-induced shear strength reduction on the dam permanent displacements.

1. Introduction

The effects of earthquakes on earth dams are documented in several post-event reconnaissance reports and studies (e.g. Wieland, 2003, Wieland, 2012; Chen et al., 2014). The rare cases of dam failures during or immediately after a seismic event were mostly caused by large earthquakes and frequently ascribed to the occurrence of liquefaction in the foundation or embankment soils (e.g. Seed et al., 1975; Wieland and Chen, 2009, JCOLD, 2012). Conversely, permanent displacements and distortions, soil mass movements and crack development have been widely observed even for moderate events without the occurrence of soil liquefaction (e.g. Harder et al., 1998; Catalano et al., 2013).

In the last 30 years the construction of new dams in Italy has been limited while the demand of water has significantly increased pointing out the need of maintaining operative the existing plants as long as possible. Among the 534 (updated to 2019) Italian large dams (height greater than 15 m or reservoir volume greater than 1 million m^3) about 300 are currently in operation. These are mainly zoned dams with an impervious core and more than 50% of them are located in areas of medium to high seismicity according to the most recent probabilistic seismic hazard (*PSHA*) assessment available for Italy (Stucchi et al., 2011) and adopted in the Italian Building Code (NTC18, 2018) and in the NTD14 (2014).

However, most of these dams were built before the establishment of a seismic code or in a period when the seismicity of the dam sites was approximately assessed and thus frequently underestimated or even entirely overlooked. As a consequence, many earth dams currently in operation in Italy have not been designed to resist earthquakes or have been designed with reference to seismic actions lower than those which would be estimated nowadays. For the few dams designed accounting

* Corresponding author.
E-mail address: ecascone@unime.it (E. Cascone).

https://doi.org/10.1016/j.enggeo.2020.105954
Received 6 May 2020; Received in revised form 15 September 2020; Accepted 3 December 2020
Available online 8 December 2020

for seismic actions, the conventional pseudo-static approach has been used to assess the overall stability conditions of the embankment with seismic coefficients ranging from 0.04 to 0.1 g depending on the first national seismic zonation dated 1974. Accordingly, the actual dynamic nature of ground motion and its effects on the dam response have not been properly accounted for.

Recently, the Italian Working Group ITCOLD "*Behaviour of dams subjected to earthquakes*" (Catalano et al., 2013) detected the 100 Italian large dams (construction period 1901–1994) that have been probably subjected to the highest levels of seismic shaking during their life (observational period 1919–2009).

For a subset of 30 dams, Catalano et al. (2013) provide results of survey activities carried out soon after severe earthquakes. Only 3 dams, located at epicentral distances R_{ep} = 2.2 to 38 km, suffered relevant damages reaching an ultimate limit state during earthquakes with magnitude M = 5.41–6.41. For 8 dams, struck by earthquakes with magnitude M = 5.41–6.43, located at epicentral distances R_{ep} = 3.7–18.6 km, the recorded or estimated peak horizontal acceleration at the dam site is $a_{h,max}$ = 0.09 *g*-0.31 *g* and only operational limit states were detected during the post-seismic survey activities. For the remaining 19 earth dams (R_{ep} = 1.1–30.5 km), subjected to earthquakes of magnitude M = 5.0–6.48 ($a_{h,max}$ = 0.07 *g* - 0.32 *g*), the post-event survey activities revealed a satisfactory seismic performance without the occurrence of significant damages.

For most of the 100 dam sites the *PSHA* provides values of the peak horizontal acceleration a_g expected on a free-field rock outcropping with time-averaged shear wave velocity in the upper 30 m $V_{s,30} \geq 800$ m/s (i.e. soil class *A*) substantially larger than those actually experienced by (or estimated for) the considered set of dams. As an example, with reference to the collapse limit state (mean return period T_R = 1950 years) the 50th percentile of a_g exceeds 0.3 *g* at 72 sites and 0.4 *g* at 36 sites, and for 8 dams it is $a_g > 0.5$ *g*; site effects could even amplify a_g leading to larger values of horizontal peak ground acceleration expected at the dam site.

Then, despite the overall positive field evidence above described, the evaluation of the seismic safety and post-seismic serviceability of Italian large dams is of paramount interest and concern. This assessment should be addressed using current seismic design criteria and modern methods of dynamic analysis to detect deficient dams which are to be rehabilitated.

Screening-level analyses of the seismic behaviour of earth dams are usually performed estimating the earthquake-induced permanent displacements through simplified Newmark-type computations. These involve conventional coupled or uncoupled rigid-block sliding analysis and coupled stick-slip analysis accounting for soil compliance and non-linear soil behaviour.

This paper describes the procedures adopted to evaluate the seismic performance of an existing zoned earth dam, accounting for updated seismic scenarios and assessing the effect of earthquake-induced shear strength reduction in the materials of the dam.

Following the prescriptions of the Italian seismic codes for dams (NTD14, 2014; NTD18, 2018) and ICOLD (2001) guidelines, assessment of the seismic response of the dam is performed defining different seismic scenarios and input motions for different limit states and using different methods of analysis, these including finite-difference (FD) pseudo-static analyses, coupled and de-coupled Newmark-type analyses and non-linear FD dynamic analyses.

This study aims to provide the selection criteria of the input motions, compare different simplified procedures to evaluate the seismic-induced dam displacements, pointing out the relevant role of the possibly occurring soil shear strength reduction, and present an improvement of the well-known Makdisi & Seed procedure, to account for the influence of non-linear soil behaviour in the evaluation of permanent displacement of the dam.

The seismic scenarios were defined using data of historical seismicity and results of the latest probabilistic seismic hazard analysis available for the dam site; the input motions were selected using compatibility criteria, based on the energy and frequency content, with the target ground motions expected at the site and aimed to match target spectra in the range of vibration periods relevant for the non-linear response of the dam.

Seismic resistance of the dam was evaluated through FD analyses performed using increasing values of the seismic coefficient until a well-defined plastic mechanism developed in the numerical model.

Earthquake-induced dam displacements were then evaluated highlighting the need of using empirical predictive relationships in which the energy content of seismic shaking is accounted for together with its duration. Computed displacements were compared with threshold values of crest settlements identified by a critical review of more than 90 case histories of dams struck by large earthquakes (Aliberti et al., 2019).

The analyses results provided a first estimate of dam performance under severe earthquake loading and permitted to identify the most critical seismic inputs to be used in advanced non-linear dynamic analyses (Cascone et al., 2021).

2. Dam description and geotechnical characterisation

Fig. 1 a,b shows a plan view of the zoned earth dam considered in this study and the main cross-section of the embankment; it is the San Pietro dam, built between 1958 and 1964 in Campania, Italy, along the river Osento. The dam embankment has a volume of about 2.2 Mm^3 and retains 17.7 Mm^3 of water with a freeboard of 2 m at the maximum impounding level of the reservoir. In its main cross-section the dam is 48 m high above the foundation level and has a base width of about 250 m; the crest is 450 m long and 9 m wide. The slope of the upstream shell of the embankment varies from about 29% to about 59%, becoming steeper towards the dam crest, while the slope of the downstream shell is equal to about 48%.

The dam core is made of low plasticity clayey silts, while the shells consist of coarse-grained soils. A 1.6 m thick coating, made of 1 m of rockfill, 0.3 m of gravel and 0.3 m of sand, protects the upstream shell from erosion due to changes in water level. Two sub-vertical filters separate the clayey core from the shells.

The foundation soils consist of a layer of alluvial soils, with an average thickness of about 7 m under the dam centre line, overlying deeper stiff overconsolidated flysch and siliceous sandstone formations. The alluvial soil underneath the dam was treated with low-pressure concrete injections to reduce the layer permeability. The seepage flow through the alluvial layer underlying the embankment is prevented by an impervious concrete diaphragm, about 16 m deep, extending along the centre line of the dam.

Before construction of the dam, 4 exploration wells 5–10 m deep, and 23 boreholes 20–60 m deep were bored in the foundation soils and undisturbed soil samples were retrieved to perform laboratory tests. However, owing to the uncertainties inherent the evaluation of the strength and stiffness parameters of the foundation and embankment soils at the time of the dam project, supplementary geotechnical investigations consisting of in situ and laboratory tests were planned by Calabresi et al. (2004) to define a reliable geotechnical model. Location of boreholes and in situ tests is shown in Fig. 1a, while Fig. 1b shows the results of in situ tests carried out in cross Sections 1 and 2, these consisting of cross-hole (*CH*), cone penetration (*CPT*), continuous dynamic cone penetration (*DP*) and standard penetration (*SPT*) tests. Laboratory tests on undisturbed samples included, in addition to standard drained and undrained triaxial compression tests, resonant column (*RC*) and bender elements (*BE*) tests, performed to evaluate the small-strain shear stiffness.

The soil profile and the geotechnical characterisation obtained from the supplementary investigations (Calabresi et al., 2004) are summarised herein.

The core of the dam mainly consists of sandy silt and clay (32% of clay, 34% of silt and 33% of sand) characterised by values of the liquid limit, plastic and consistency indexes W_L = 42.3%, PI = 21.5% and I_C = 0.8–1.1, respectively, while the shells consist of sandy gravel (53% of gravel, 24% of sand, less than 13% of clay and silt).

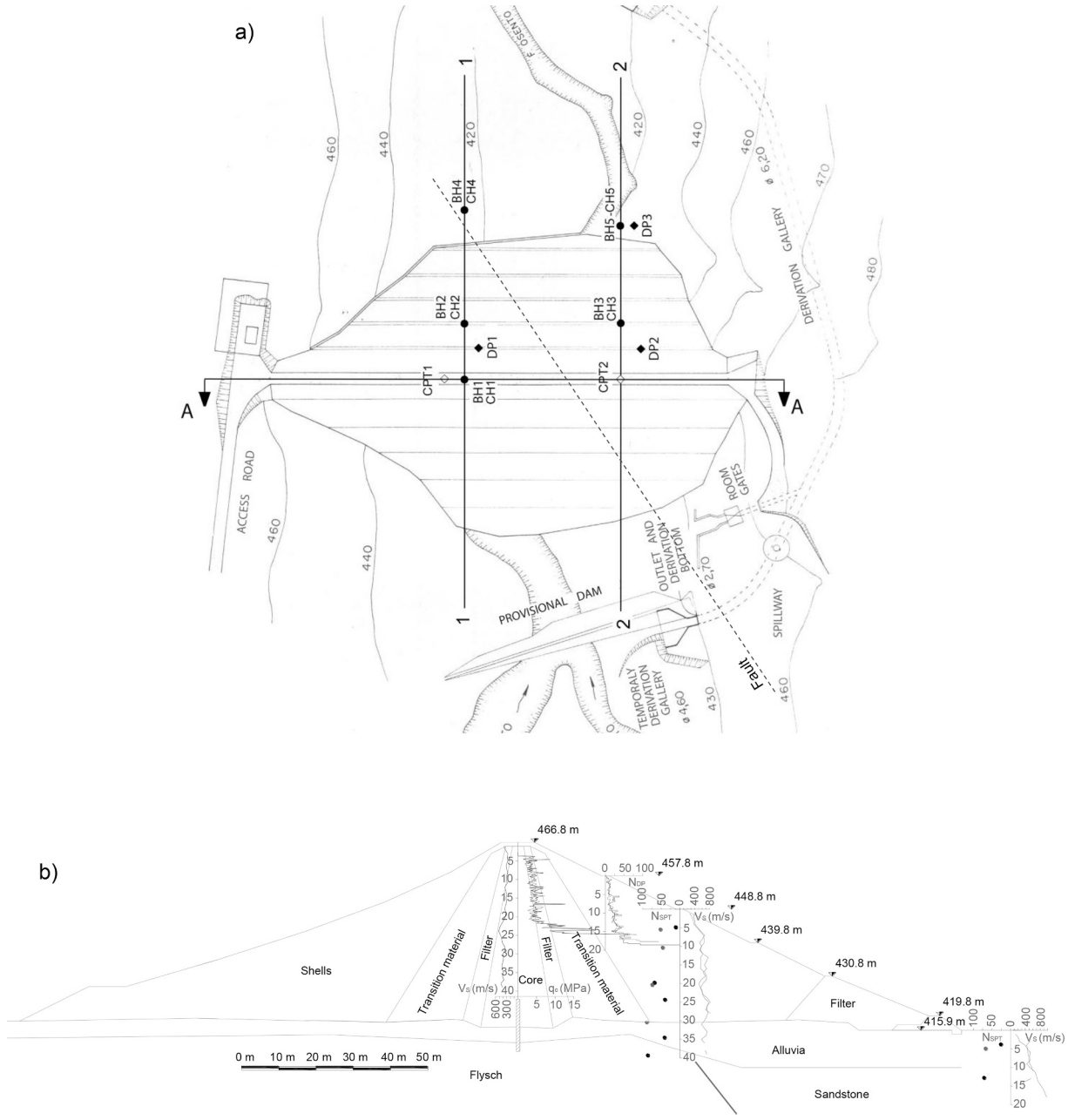

Fig. 1. San Pietro dam: a) plan view and location of geotechnical investigations; b) cross section of the dam (adapted from Calabresi et al., 2004).

The relative density of the coarse-grained soils of the shells was estimated from in situ penetration tests, using the empirical relationships proposed by Gibbs and Holtz (1957), Skempton (1986) and Kulhawy and Mayne (1990). The computed values of D_R are plotted against the vertical effective stress in Fig. 2a–c, together with the average profiles and the profiles corresponding to the 16th and 84th percentile of the data distribution. Despite the scattering in the data, which is usual at shallow depths in well graded granular soils, the comparison of the average profiles shows values of D_R varying in the range 45–65% in the upper portion (depth less than about 20 m) and increasing up to about 75% at greater depths. According to the data given in Fig. 2, cyclic reduction of the shear strength due to the possible occurrence of pore water pressure build-up could affect the seismic performance of the dam.

Table 1 lists the effective cohesion c' and the angle of shearing resistance φ' as obtained from laboratory and in situ tests.

The profiles of the small-strain shear modulus G_0 obtained from the cross-hole tests carried out in the core (*CH1*), in the shells (*CH2*, *CH3*) and in the foundation soil downstream of the dam (*CH4*, *CH5*), are shown in Fig. 3a. The scatter observed for G_0 in the shells can be ascribed to the above mentioned scatter of the relative density (Fig. 2) obtained at the end of construction at the different locations of the downstream shell, where tests *CH2* and *CH3* were carried out (Fig. 1). The two sets of data given for the Alluvia refer to cross hole tests performed under (*CH3*) and aside (*CH4*, *CH5*) the dam embankment at very different effective stresses. A stiff bedrock can be identified at the depth where the flysch and sandstone formation is encountered since G_0 increases with depth starting from about 1350 MPa and the shear wave velocity is always larger than about 820 m/s.

Resonant column tests were also performed on an undisturbed sample retrieved in the core at a depth of 15 m from the crest. The normalised shear modulus G/G_0 and the excess pore water pressure ratio $\Delta u^* = \Delta u/p'_0$, with p'_0 equal to the in situ mean effective stress, are plotted in Fig. 3b as a function of the shear strain amplitude γ. Conversely, no experimental data are available for the variation of the

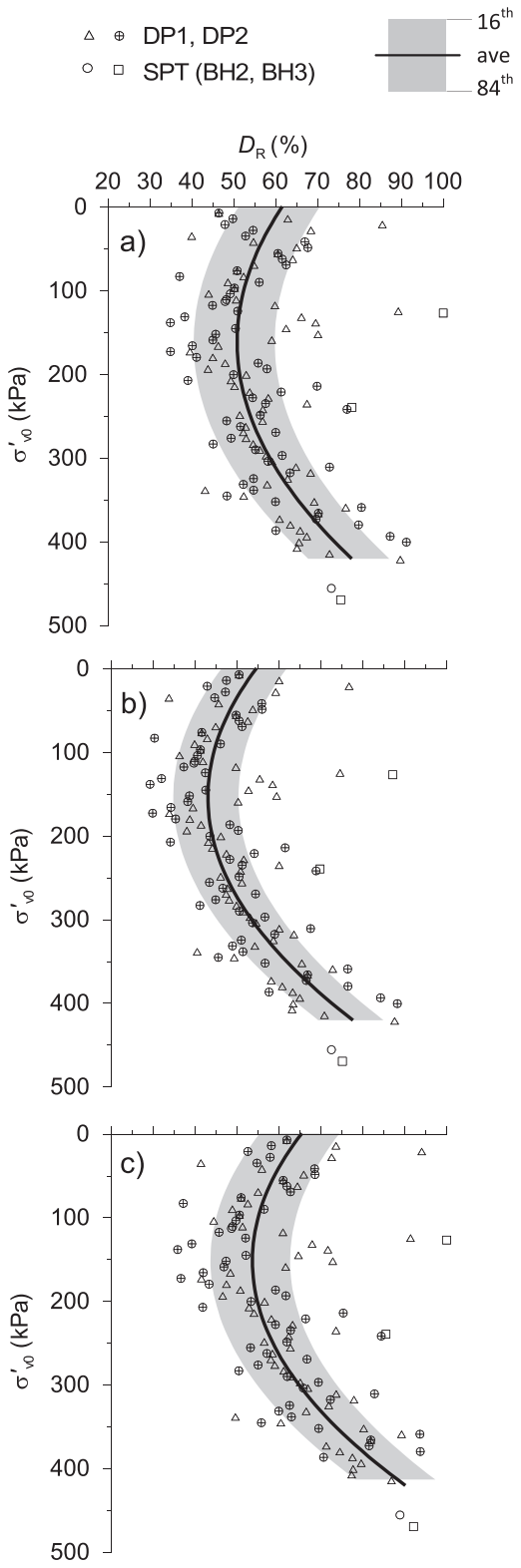

Fig. 2. Profiles of soil relative density obtained from in situ test results using empirical relationships: a) Gibbs and Holtz (1957); b) Skempton (1986); c) Kulhawy and Mayne (1990)

damping ratio with γ.

In Fig. 3b the curves proposed by Vucetic and Dobry (1991) for values of plasticity index PI = 15, 30 and 50% are also represented showing the best agreement with the curve at PI = 50%, despite the soil samples retrieved from the core of the dam are characterised by an average value of PI = 21.5%.

For $\Delta u^* = 5\%$ a volumetric threshold $\gamma_v \cong 0.03\%$ is evaluated, that is consistent with the data provided by Hsu and Vucetic (2006) for silts and clays having PI in the range 14–30%.

Table 1
Shear strength parameters obtained from in situ and laboratory tests.

Soil	Test	c' (kPa)	φ' (°)
Shells	TX-CID [a]	0	36
	DP, SPT	–	35–40
	TX-CIU, CID	30	27
Alluvia	DP, SPT	–	40 ÷ 45

[a] large samples (diameter 80 mm, height 160 mm).

3. Limit states and indexes of seismic performance

In the last decades, performance-based approaches have been introduced to evaluate the seismic behaviour of geotechnical systems and to estimate the financial and social risk associated to irreversible damages or failures induced by earthquakes. In this context, appropriate performance indexes must be introduced, and suitable threshold values must be defined, that identify the attainment of limit states associated to different seismic scenarios.

According to international standards (e.g. ICOLD, 2001, 2010), the seismic performance of dams must be checked to verify that stability and serviceability conditions are warranted against expected ground motions characterised by either a relatively low or a high probability of occurrence during the dam's life-cycle. This to avoid catastrophic failures and uncontrolled release of water during extreme (low probable) events and to ensure operational conditions of the dam and related facilities during less severe (highly probable) earthquakes.

According to these principles, the Italian seismic code for dams (NTD14, 2014) introduces four limit states to be checked: two serviceability (*Operational Limit State, OLS,* and *Damage Limit State, DLS*) and two ultimate (*Life Safety Limit State, LLS,* and *Collapse Limit State, CLS*) limit states that can be attained depending on the loss of a characteristic condition defined by the level of damage induced by earthquake loading and the occurrence of uncontrolled release of water.

As described in Table 2, an *Operational Limit State* (*OLS*) is achieved when the operating condition is lost due to the occurrence of repairable damages which, however, do not lead to uncontrolled release of water. When the damages are unrepairable, a *Damage Limit State* (*DLS*) is attained if uncontrolled release of water does not occur; otherwise, a *Life Safety Limit State* (*LLS*) is attained if the dam does not collapse, while a *Collapse Limit State* (*CLS*) is achieved if an overall failure mechanism develops (Table 2). It is worth mentioning that the limit condition to be lost for the achievement of the *LLS* is in a good agreement with the performance criteria introduced by ICOLD (2010) with reference to the *Safety Evaluation Earthquake* (*SEE*); similarly, the limit conditions corresponding to the achievement of the *OLS* and the *DLS* fit well with the performance criteria associated with the *Operating Basis Earthquake* (*OBE*).

However, as shown in next sections, values of the mean return period prescribed by the Italian codes to define the design earthquakes for each limit state are different from those suggested by ICOLD (2010).

According to (Swaisgood, 2003) and (Ishihara, 2010) the crest settlement u_c can be assumed as a reliable index of seismic performance since it is representative of the overall seismic response of the dam and is suitable for the evaluation of the level of earthquake-induced damage. In this vein, through a systematic review of a large set of data, related to 90 well documented case histories of earthquake-induced damages to various kinds of dams and related facilities, Aliberti et al. (2019) defined threshold values of u_c to be used as possible reference indexes in performance-based seismic analyses of dams. Using some engineering judgment, damage description available for each case history was

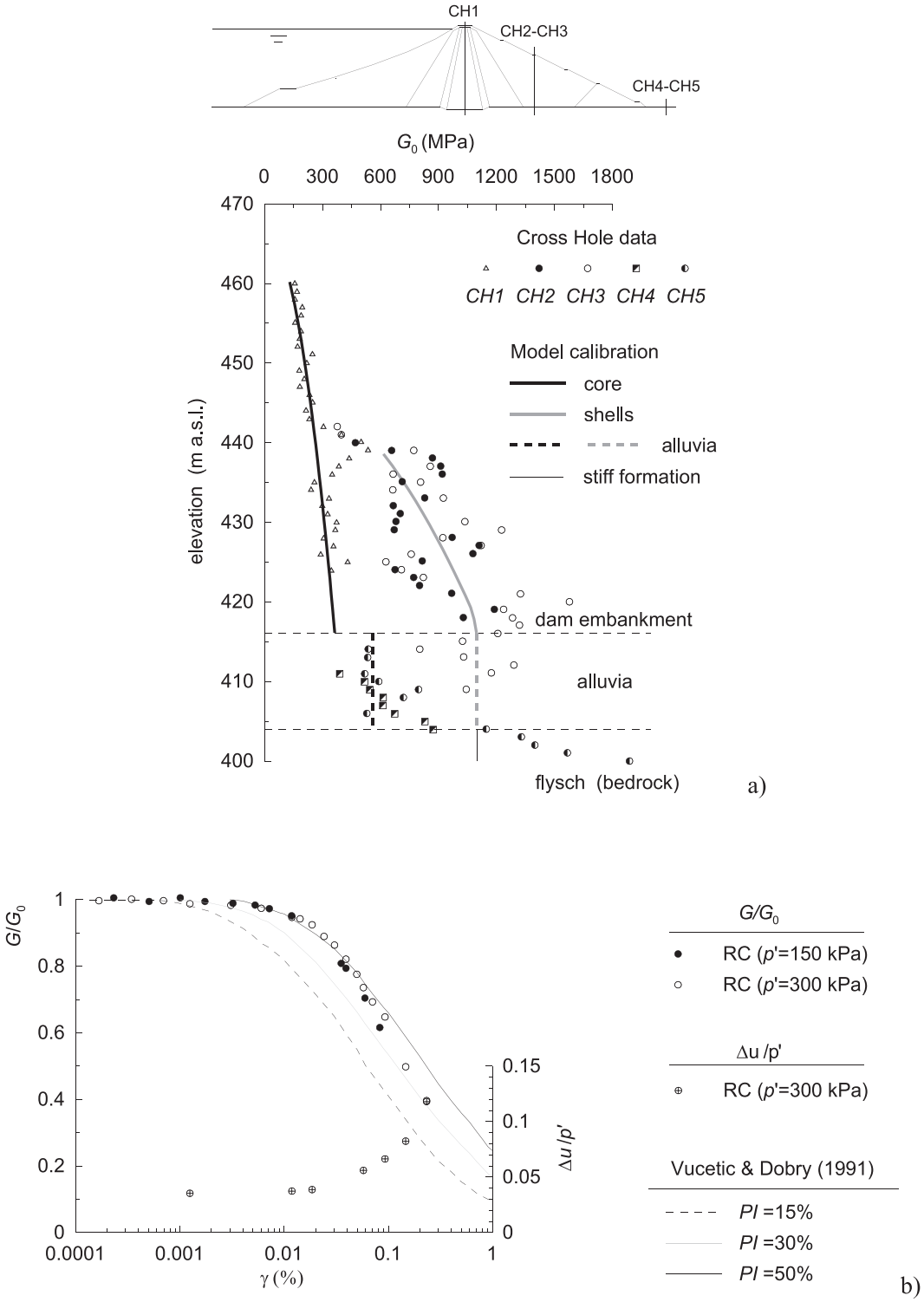

Fig. 3. a) Profiles of small strain shear modulus G_0 obtained from *CH* tests and best fits adopted in the numerical model; b) *RC* test results and data from literature (Cascone et al., 2021)

classified in four classes and examined to relate the achievement of one of the limit states described in Table 2 together with the corresponding threshold values of the crest settlement ratio $(u_c/H)_y$ where $H = H_d + H_f$ is the height of the dam H_d plus the thickness of the deformable foundation soils H_f. Specifically, a *none*, *minor*, *moderate* and *serious* level of damage (*DL*) was defined by Aliberti et al. (2019) and associated to threshold values of $(u_c/H)_y$ = 0.1%, 0.4%, 1.25% and 2.5%, these corresponding to the occurrence of *OLS, DLS*, *LLS* and *CLS*, respectively. In addition, the seismic stability of the dam must also be checked verifying that the freeboard is greater than crest settlement for each limit state (Table 2).

Table 2
Limit states introduced by the *Italian Code for Dams* (NTD14, 2014), parameters of the probabilistic seismic hazard assessment prescribed by the *Italian Building Code* (NTC18, 2018) for the site of San Pietro Dam and indexes of seismic performance (Aliberti et al., 2019).

Characteristic /Limit condition: to be lost for / to be attained for the achievement of the limit state	No damage occurs in the dam and in the plant facilities	Occurrence of repairable damages which do not lead to uncontrolled release of water	Occurrence of unrepairable damages which do not lead to uncontrolled release of water	Occurrence of unrepairable damages which produce uncontrolled release of water and/or risk of loss of human life	Dam collapse

Limit state		*Operational limit state (OLS)*	*Damage limit state (DLS)*	*Life safety limit state (LLS)*	*Collapse limit state (CLS)*
Limit conditions and performance index		$u_c/H < (u_c/H)_y = 0.1\%$ $u_c <$ freeboard	$u_c/H < (u_c/H)_y = 0.4\%$ $u_c <$ freeboard	$u_c/H < (u_c/H)_y = 1.25\%$ $u_c <$ freeboard	$u_c/H < (u_c/H)_y = 2.5\%$ $u_c <$ freeboard
P_{VR} (%)		81	63	10	5
T_R (years)		60	101	949	1950
F_o		2.501	2.494	2.371	2.357
a_g (g)	16th	0.0636	0.0884	0.2405	0.3114
	50th	0.0744 (0.078)*	0.0979 (0.101)*	0.2860 (0.304)*	0.3920 (0.414)*
	84th	0.0853	0.1185	0.3389	0.4641

(*) evaluated for the node (ID 32331) of the reference grid closest (3.4 km) to the site of the dam.

4. Historical seismicity and probabilistic seismic hazard

4.1. Seismic history of the dam site

Seismic historical data for the site of San Pietro dam were selected from the Italian Macroseismic Database DBMI15 v1.5 (Locati et al., 2016) that reports macroseismic intensity information of the earthquakes occurred in Italy from 1000 until 2014.

Fig. 4 a,b shows the MCS epicentral macroseismic intensity I_0 and the corresponding Moment Magnitude M_w (estimated for most events) of the earthquakes which were felt, with an observed intensity I, in the five municipalities closest to the dam ($D < 10$ km): Aquilonia Vecchia ($D \approx 1.3$ km), Monteverde ($D \approx 2.7$ km), Aquilonia ($D \approx 2.8$ km), Monticchio Bagni ($D \approx 8.3$ km) and Lacedonia ($D \approx 8.5$ km). Data of Fig. 4 a,b refer to 42 earthquakes, occurred between 1456 and 2006, with $I_0 = 4 \div 11$ MCS and $M_w = 3.71 \div 7.19$, which were felt in the selected five municipalities with an intensity $I = 3 \div 10$ MCS.

The oldest documented event, the Molise 1456 earthquake, is also the largest event ($I_0 = 11$ MCS, estimated $M_w = 7.19 \pm 0.10$) listed in the DBMI15, with an epicentral distance $R_{ep} \approx 74.3$ km of the dam site and an observed intensity $I = 9$ MCS at the closest municipality of Aquilonia Vecchia ($D \approx 1.3$ km). Other two events of similar intensity occurred in the same time-interval: the 1857 Basilicata earthquake ($I_0 = 11$ MCS, estimated $M_w = 7.12 \pm 0.10$, $R_{ep} \approx 77.5$ km), with an observed intensity $I = 9$ MCS at Aquilonia Vecchia, and the 1915 Marsica earthquake ($I_0 = 11$ MCS, estimated $M_w = 7.08 \pm 0.08$, $R_{ep} \approx 199$ km), with $I = 4$–5 MCS at Aquilonia ($D \approx 2.8$ km). These three large events ($M_w \approx 7.1$–7.2) can be identified as far-field ground motions having distances $R_{ep} \approx 74$–199 km.

Conversely, the near-field events relevant to the dam site are the 1934 Irpinia-Basilicata earthquake ($I_0 = 10$ MCS, estimated $M_w = 6.81 \pm 0.10$, $R_{ep} \approx 25.6$ km) and the 1930 Irpinia earthquake ($I_0 = 11$ MCS, estimated $M_w = 6.67 \pm 0.08$, $R_{ep} \approx 17.3$ km) which were observed with $I = 7$ MCS at Aquilonia ($D \approx 2.8$ km) and $I = 10$ MCS at Aquilonia Vecchia ($D \approx 1.3$ km), close to the dam.

During dam construction (1958–1964) the site was struck by the 21 August 1962 Irpinia earthquake ($I_0 = 11$ MCS).

After the end of dam construction (1964–2006), 19 relevant events occurred with $I_0 = 5$–10 MCS and $M_w = 3.7$–6.8. The largest of these events is the 1980, $M_W = 6.81$, Irpinia earthquake ($I_0 = 10$ MCS), the highest magnitude seismic event recorded in Italy since 1915, which caused severe damage, casualties (about 3000 dead, 9000 injured and 200,000 homeless) and landslides in a wide region. Despite the large intensity observed at the site of interest ($R_{ep} \approx 26$ km, $I = 7$ MCS at Lacedonia) and the long duration (about 80 s) of the main shock, no significant damage was observed in the dam.

Based on these historical data, events with $M_w = 6.8$ to 7.1 can be considered to define the maximum credible earthquake (*MCE*) for San Pietro dam.

4.2. Probabilistic seismic hazard analysis

The expected ground motion was assessed through a probabilistic seismic hazard analysis (Stucchi et al., 2011). For a 0.05° grid of points with a spacing of 5 km and for reference site conditions of horizontal outcropping bedrock with a time-averaged shear wave velocity, $V_S \geq 800$ m/s, the *PSHA* is described by the horizontal peak ground acceleration a_g, the uniform hazard spectral acceleration S_a and the results of the M_w-R_{jb}-ε deaggregation analysis for the 50th percentile of a_g, where M_w is the earthquake moment magnitude, R_{jb} is the Joyner and Boore (1981) site-to-source distance and ε is the Gaussian variable introduced by Bazzurro and Cornell (1999).

Values of a_g are available for mean return periods T_R of 30 to 2500 years; the spectral acceleration S_a (available for $T = 0.1$–2 s) and the results of the deaggregation analysis (bins of width 0.5 in magnitude and 10 km in distance) including the mean values of M_W, R_{jb} and ε, are available for exceedance probabilities of 2% to 81% in 50 years (P_{50}).

Fig. 4c shows a detail of the Italian seismic hazard map (Stucchi et al., 2011) relevant to the 50th percentile of horizontal peak ground acceleration a_g expected for $T_R = 475$ years ($P_{50} = 10\%$). Starting from the data available for the four nodes of the reference grid enclosing the site of San Pietro dam, the parameters derived from the *PSHA* (a_g, S_a and M_w-R_{jb}-ε deaggregation analysis) were averaged using the site-to-node distances as weights. The outcrop acceleration a_g is plotted in Fig. 4d against T_R: the median values (50th percentile) of a_g are shown in the figure together with the 16th and 84th percentiles of the seismic hazard distribution. Values of a_g corresponding to each of the limit states prescribed by the Italian codes (§ 3) can be estimated using Fig. 4d.

Results of the M_w-R_{jb}-ε deaggregation analysis are summarised in Fig. 5a,b where the thick black lines represent the mean values of M_w (Fig. 5a) and R_{jb} (Fig. 5b) against the mean return period T_R: $M_{w,ave}$ varies from 5.65 ($T_R = 30$ years, $P_{50} = 81\%$) to 6.21 ($T_R = 2475$ years, $P_{50} = 2\%$), while the corresponding average distances $R_{jb,ave}$ are equal to 32.4 km and 7.2 km. The moment magnitudes, $M_w = 6.8$ and 7.1 detected from seismic historical data for the possible *MCE*s are plotted for comparison in Fig. 5a with dashed lines. In Fig. 5b the limit of near-field motions considered in FEMA (2005) is also represented. The shaded areas depicted in Fig. 5a,b envelope the ranges of magnitudes M_w and distances R_{jb} corresponding to the highest contribution to the

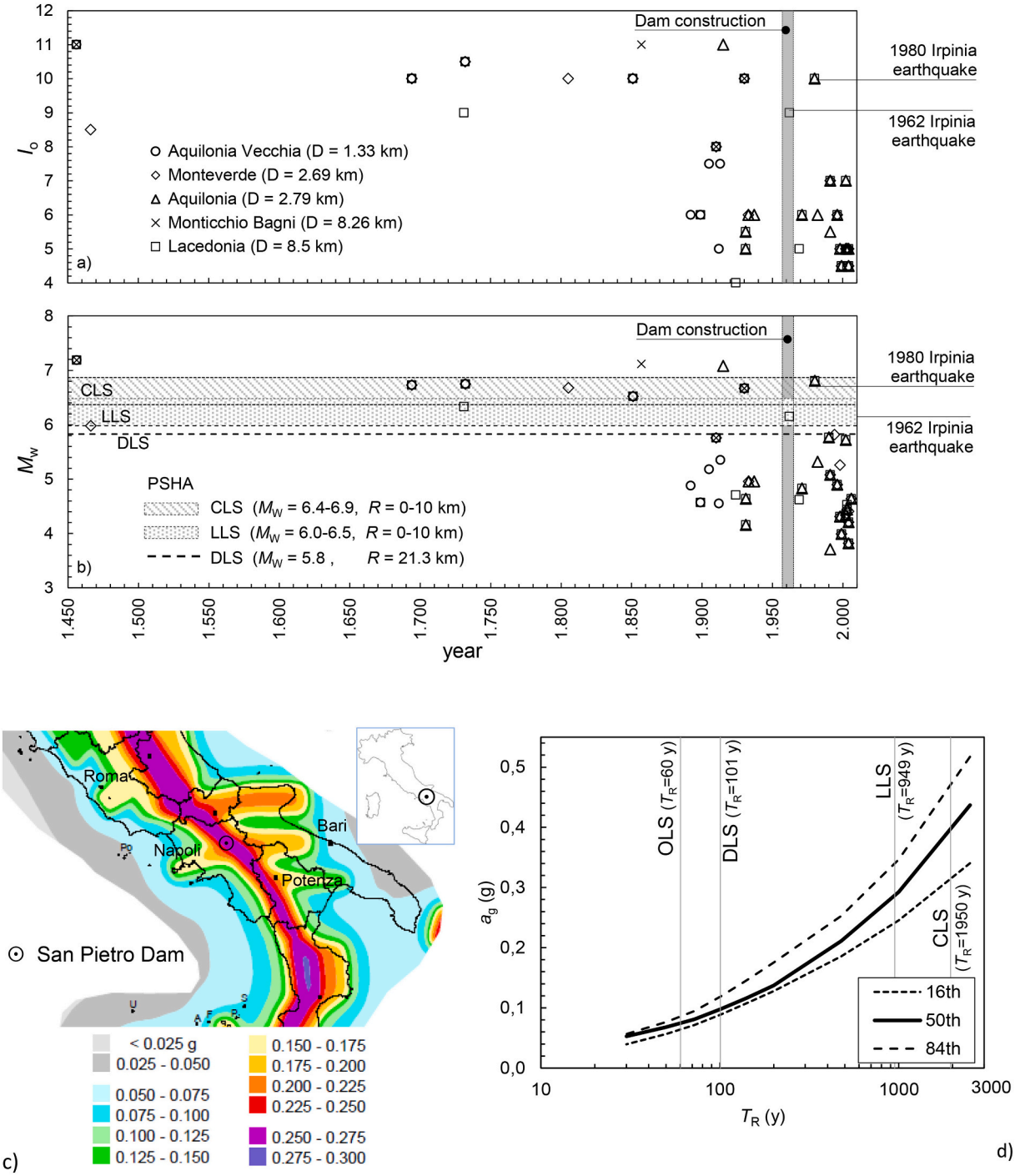

Fig. 4. Seismic historical data (a,b) and seismic hazard deaggregation analysis (c,d) for the dam site: a,b) epicentral macroseismic intensity (MCS scale) and moment magnitude of the events felt in five municipalities closest ($D < 10$ km) to the dam (time interval 1456–2006); c) detail of the Italian seismic hazard map giving the 50th percentiles of a_g for $T_R = 475$ years; d) values of a_g versus the mean return period T_R.

seismic hazard at the dam site for return periods $T_R > 100$ years: $M_{w,max}$ varies from 4.5÷5.0 ($T_R = 101$ years, $P_{50} = 39\%$) to 6.5÷7.0 ($T_R = 2475$ years, $P_{50} = 2\%$). Concurrently, it is always $R_{jb,max} = 0$–10 km. Again, Fig. 5a,b provide pairs of M_w-R_{jb} for the limit states prescribed by the Italian codes.

5. Selection of input motions

5.1. Target input motions

The severity of the seismic actions to be adopted for assessing the seismic performance of existing dams depends on the probability of occurrence P_{VR} of an earthquake during a specific time interval V_R, which is related to the dam relevance for the post-seismic emergency plans, and to the number of years during which, under regular maintenance, the dam can be used for its original design purpose. According to

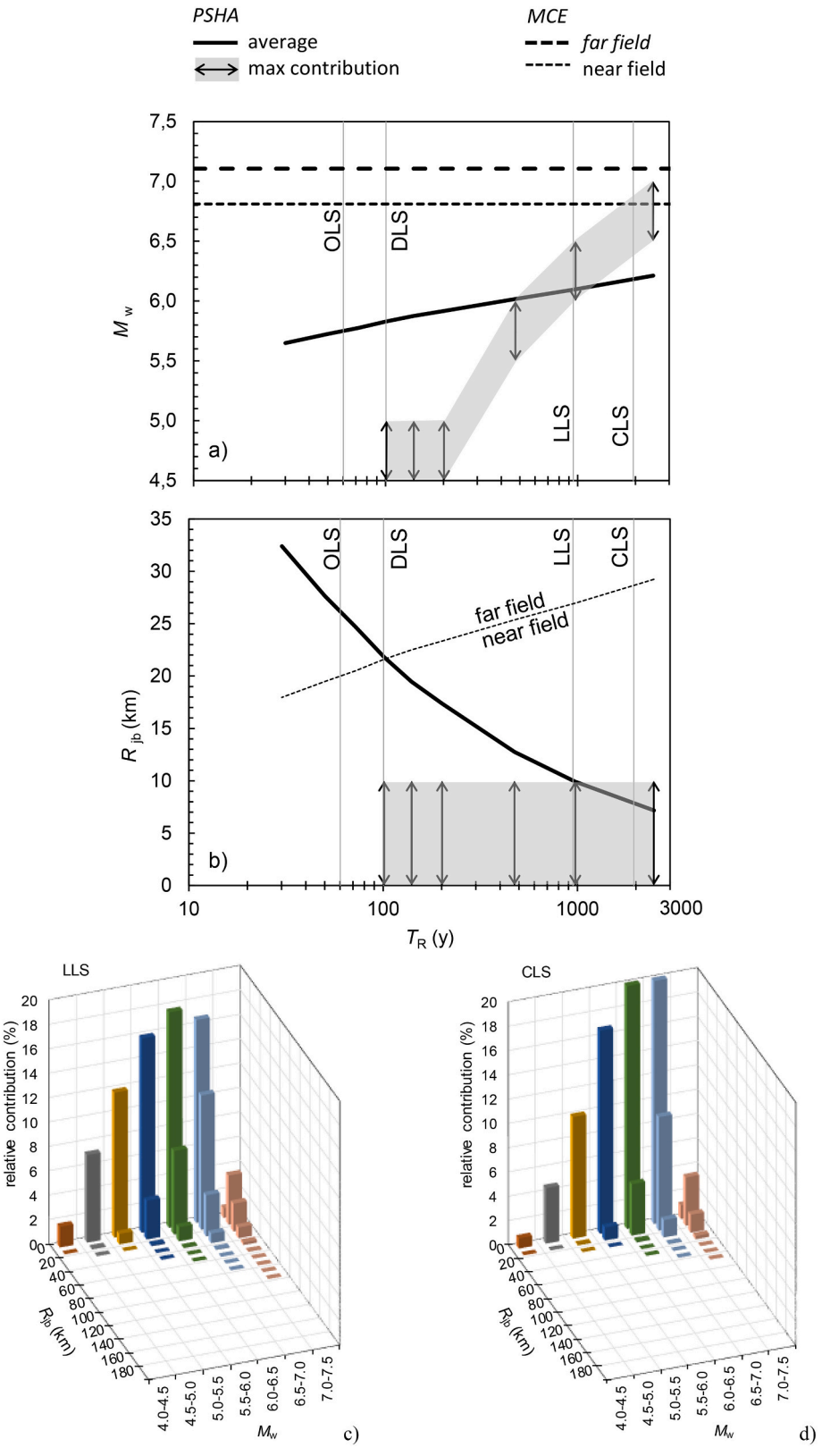

Fig. 5. Results of the M_w-R_{JB}-ε deaggregation analysis of a_g at the dam site.

the mandatory prescriptions of the Italian codes (NTD14, 2014; NTC18, 2018), $V_R = 100$ years was assumed for the seismic analyses.

For each of the prescribed limit states, Table 2 lists the values of P_{VR}, the corresponding values of the return period T_R, the values of the amplification factor F_o of the maximum spectral acceleration and the 50th percentile values of a_g provided by the *PSHA*. The mean values of a_g detected at the node of the reference grid closest to the dam site (ID 32331) are also listed in Table 2.

For the two serviceability limit states, T_R is equal to 60 (*OLS*) and 101 (*DLS*) years and a_g is equal to 0.074 *g* and 0.098 *g* (0.078 *g* and 0.101 *g* at node ID 32331 – Table 2); values of a_g corresponding to 16th and 84th percentiles provide a variability of the mean estimate of about −14% to +21%. For the two ultimate limit states (*LLS* and *CLS*) the mean return periods are $T_R = 949$ and 1950 years, with $a_g = 0.286$ *g* and 0.392 *g* (0.304 *g* and 0.414 *g* at node ID 32331 – Table 2) and are included in the following intervals of variation for 16th and 84th percentiles: 0.240 *g*-0.339 *g* for *LLS* and 0.311 *g*-0.464 *g* for *CLS*.

It is worth mentioning that, regardless the probability of occurrence of the earthquake in the time interval V_R considered to describe the severity of the seismic actions, for dams whose failure presents a great social hazard, ICOLD (2010) suggests $T_R = 145$ years for the *Operating Basis Earthquake* (*OBE*), whose definition is close to the *OLS* and *DLS*, and $T_R = 3000 \div 10.000$ years for the *Safety Evaluation Earthquake* (*SEE*) characterised by the same limit conditions required to attain the *LLS*.

Herein, only the ultimate limit states (*LLS* and *CLS*) were considered for the seismic analysis of the dam: estimated values of $a_g = 0.304$ *g* and 0.414 *g* were used as targets for the *LLS* ($T_R = 949$ years) and the *CLS* ($T_R = 1950$ years) to select the input motions to be adopted in the numerical analyses (Fig. 4d, Table 2) that were defined in terms of horizontal and vertical acceleration time-histories. Suitable ranges of moment magnitude (M_w) and Joyner and Boore (1981) distance (R_{jb}) were defined to select the seismic records using the data obtained from the historical seismicity (Fig. 4a,b) and seismic hazard deaggregation analysis (Fig. 5a,b). Specifically, the distribution of the contribution of each pair M_w-R_{jb} and the corresponding mean ($M_{w,ave}$-$R_{jb,ave}$) and maximum ($M_{w,max}$-$R_{jb,max}$) values were estimated to detect the M_w-R_{jb} groups that dominate the seismic hazard at the dam site. Similarly, the return periods corresponding to the two ultimate limit states and the uniform hazard response spectra for the site of the dam were evaluated.

Fig. 5c,d shows the computed results in terms of deaggregation plots. The deaggregation plots for the *LLS* ($T_R = 949$ years, Fig. 5c) and the *CLS* ($T_R = 1950$ years, Fig. 5d) provide the ranges of both M_w and R_{jb} that dominate the seismic hazard at the dam site, thus identifying the scenario earthquakes for San Pietro Dam. Specifically, $M_{w,max} = 6.0$–6.5 and $M_{w,max} = 6.4$–6.9 were assumed for the *LLS* and *CLS*, with values of $R_{jb,max} = 0$–10 km.

5.2. Selection criteria and results

The input motions were selected using an Italian, ITACA 2.1 (Luzi et al., 2016), and an international (PEER, 2016) database of seismic records. A first selection of acceleration time-histories was carried out setting $M_w = 6.5 \pm 0.5$ and 1 km $\leq R_{jb} \leq$ 25 km for both the *LLS* and *CLS*. The selection was further refined focusing on the horizontal records, checking the similarity between the elastic response spectrum of the acceleration time histories and the target spectrum (Bommer and Acevedo, 2004; Pagliaroli and Lanzo, 2008).

The spectra defined by the Italian seismic code (NTC18, 2018) were considered as targets for the two ultimate limit states. Compatibility of selected acceleration records was checked in terms of amplitude and frequency content, through the response spectra. To this purpose a scale factor *F* and two statistical parameters, R^2 and D_{rms} were used. The scale factor *F* allows ensuring compatibility in terms of peak horizontal acceleration (i.e. spectral ordinate for $T = 0$ s):

$$F = \frac{(a_{h,max})_j}{(a_{h,max})_t} \tag{1}$$

The Pearson correlation index R^2 and the average root-mean square deviation D_{rms} evaluate the deviation of the normalised response spectra of the selected records from the target spectrum in a given period interval (T_{min}-T_{max}):

$$R = \frac{N \cdot \sum_{i=1}^{N} \overline{S}_{a,t}(T_i) \cdot \overline{S}_{a,j}(T_i) - \sum_{i=1}^{N} \overline{S}_{a,t}(T_i) \cdot \sum_{i=1}^{N} \overline{S}_{a,j}(T_i)}{\sqrt{\left\{ N \cdot \sum_{i=1}^{N} \left[\overline{S}_{a,t}(T_i)\right]^2 - \left[\sum_{i=1}^{N} \overline{S}_{a,t}(T_i)\right]^2 \right\} \cdot \left\{ N \cdot \sum_{i=1}^{N} \left[\overline{S}_{a,j}(T_i)\right]^2 - \left[\sum_{i=1}^{N} \overline{S}_{a,j}(T_i)\right]^2 \right\}}} \tag{2}$$

$$D_{rms} = \frac{1}{N} \sqrt{\sum_{i=1}^{N} \left[\overline{S}_{a,t}(T_i) - \overline{S}_{a,j}(T_i)\right]^2} \tag{3}$$

In Eqs. (1)–(3) $(a_{h,max})_j$ and $(a_{h,max})_t$ are the peak horizontal acceleration of the *j-th* record and the target ground motion, expected at the dam site on outcropping rock; $\overline{S}_{a,t}(T_i)$ and $\overline{S}_{a,j}(T_i)$ denote the normalised spectral accelerations of the target motion and the *j-th* record; *N* is the number of equally spaced ($\Delta T = 0.01$ s) periods of the response spectra in the range T_{min}-T_{max}. Coefficient R^2 was evaluated assuming $T_{min} = 0.1$ s and $T_{max} = 4.0$ s to verify the overall compatibility of selected ground motions. Conversely, since the first natural period of horizontal elastic vibration of the dam is $T_{1e} \approx 0.32$ s (Cascone et al., 2021), to select input ground motions capable to produce frequency coupling with the dam, $T_{min} = 0.1$ s and $T_{max} = 0.5$ s were assumed to evaluate D_{rms}. To obtain at least five accelerograms for each ultimate limit state, the following limits were defined for the selection parameters: $F \leq 2.0$, $R^2 \geq 0.8$ and $D_{rms} \leq 0.15$ for the *LLS* and $F \leq 2.5$, $R^2 \geq 0.8$ and $D_{rms} \leq 0.15$ for the *CLS*.

Table 3 reports the selected seismic records and the corresponding selection parameters *F*, R^2 and D_{rms}: records #3, #4 and #5 fit the adopted limitations for both the *CLS* and the *LLS*. Moment magnitude M_w of the seismic events corresponding to the selected records and the Joyner and Boore (1981) site-source distance of the recording stations are also listed in Table 3.

Time histories of horizontal acceleration $a_h(t)$ of the selected records are plotted in Fig. 6 a–g, while the Fourier amplitude spectra are shown in Fig. 6 h–p together with the first natural frequency of horizontal elastic vibration of the dam $f_{1e} = 1/T_{1e} = 3.12$ Hz. The smoothed spectra plotted with thick lines in Fig. 6 h–p show that records #1, #2, #4 and #7 are characterised by one ($f_p \approx 1.8$–2.8 Hz) or two dominant frequencies while the remaining records exhibit a broad band frequency content.

The time histories of vertical acceleration $a_v(t)$ of the selected records and the corresponding Fourier amplitude spectra are plotted in the Fig. 7a–e and Fig. 7f–n. The first natural frequency of vertical elastic vibration of the dam $f^v_{1e} = 4.54$ Hz (Cascone et al., 2021), is also plotted in Fig. 7f–n. A frequency $f_p = 2.1$–2.9 Hz substantially lower than f^v_{1e} predominates for the vertical records #1 and #2, while a broad band frequency content generally characterises the spectra of the remaining time histories of vertical acceleration.

Comparison of the target spectra for the site of San Pietro dam with the normalised response spectra of the selected horizontal records is shown in Fig. 8a–d for the CLS (Fig. 8a,b) and the LLS (Fig. 8c,d). Specifically, Fig. 8a,d compare the normalised response spectra with the 50th-percentile uniform hazard spectra computed at the dam site for the two ultimate limit states, the grey areas representing the envelope of the uniform hazard spectra defined by 16th and 84th percentiles; Fig. 8b,e compare the average normalised spectrum with the spectral shape prescribed by NTC18 (2018), the grey areas indicating the envelope of normalised response spectra of the selected records. The fundamental

Table 3
Selection criteria and main characteristics of the horizontal acceleration time histories.

CLS (T_R = 1950 years)									
$6.0 \le M_w \le 7.0$ 1 km $\le R_{jB} \le$ 25 km				$(a_{h,max})_t$ = 0.414 g $(a_{v,max})_t$ = 0.359 g					
#	Earthquake	Station, record, earthquake data	M_w	R_{jb} (km)	$a_{h,max}$ (g)	$a_{v,max}/a_{h,max}$	F	R^2	D_{rms}
1	Loma Prieta	Gilroy Array # 1, 000, 18/10/1989	6.9	8.84	0.411	0.52	1.008	0.817	0.072
2	Loma Prieta	Gilroy Array # 1, 090, 18/10/1989	6.9	8.84	0.473	0.45	0.875	0.843	0.148
3	Parkfield −02 CA	Parkfield – Turkey Flat # 1, 270, 28/09/2004	6.0	4.66	0.245	0.31	1.688	0.908	0.106
4	Parkfield −02 CA	Parkfield – Turkey Flat # 1, 360, 28/09/2004	6.0	4.66	0.196	0.38	2.111	0.900	0.095
5	Northridge	Wonderland Ave, 185, 17/01/1994	6.7	15.11	0.172	0.61	2.406	0.941	0.087
LLS (T_R = 949 years)									
$6.0 \le M_w \le 7.0$ 1 km $\le R_{jB} \le$ 25 km				$(a_{h,max})_t$ = 0.304 g $(a_{v,max})_t$ = 0.226 g					
#	Earthquake	Station, record, earthquake data	M_w	R_{jb} (km)	$a_{h,max}$ (g)	$a_{v,max}/a_{h,max}$	F	R^2	D_{rms}
3	Parkfield −02 CA	Parkfield – Turkey Flat # 1, 270, 28/09/2004	6.0	4.66	0.245	0.31	1.239	0.913	0.106
4	Parkfield −02 CA	Parkfield – Turkey Flat # 1, 360, 28/09/2004	6.0	4.66	0.196	0.38	1.550	0.888	0.099
5	Northridge	Wonderland Ave, 185, 17/01/1994	6.7	15.11	0.172	0.61	1.766	0.935	0.087
6	Iwate, Japan	IWT010, NS, 13/06/2008	6.9	16.26	0.226	0.91	1.348	0.929	0.065
7	Tottori, Japan	SMNH10, EW, 06/10/2000	6.6	15.58	0.231	0.59	1.318	0.809	0.140

vibration period of the dam, T_{1e} is also plotted in the figures. The average spectra of the selected records are in a fair agreement with the target spectra for periods $T < 0.5$ s irrespective of the limit state, while smaller spectral accelerations are estimated at larger periods.

A compatibility check for the vertical component of the selected records was also performed since the controlling *M-R* scenarios for the vertical motion may differ from those for the horizontal components (e.g. Lanzo et al., 2015; Russo et al., 2017).

The ratio of vertical to horizontal peak accelerations, $a_{v,max}/a_{h,max}$, is equal to 0.31–0.91 for the *LLS* and to 0.31–0.61, for the *CLS* (Table 3). The upper limits of these ranges are close to the ratios $a_{v,max}/a_{h,max} = 0.74$ and $a_{v,max}/a_{h,max} = 0.87$ prescribed by the Italian Building Code for the two ultimate states at the dam site. Accordingly, the target peak vertical acceleration $(a_{g,v})_t$ is equal to 0.226 *g* and 0.359 *g* for the *LLS* and the *CLS*, and the corresponding average values of the scaling factor are about 1.64 (*LLS*) and 1.55 (*CLS*).

The normalised response spectra of the vertical component of the selected records and their average are compared with the spectral shape prescribed by NTC18 (2018) for the *CLS* and the *LLS* in Fig. 8c,f; the first natural period of vertical elastic vibration of the dam, $T^V_{1e} = 1/f^V_{1e} = 0.22$ s, is also represented in the figures. Spectral compatibility of the records selected for the *CLS* appears satisfactory for periods close to T^V_{1e} with a negligible difference for $T = T^V_{1e}$, while for the *LLS* the difference around T^V_{1e} is larger, even if a conservative estimate of spectral accelerations is obtained.

For the seismic analyses described herein, all the horizontal records were scaled to the target peak ground acceleration $(a_g)_t$ estimated for the two ultimate limit states. Vertical components were scaled using the same scale factor F adopted for the corresponding horizontal components (Table 3); this yielded to ratios of the target to the adopted peak vertical accelerations in the range 0.82÷2.43 for the *LLS* and 1.42÷2.27 for the *CLS* (with the only exception of record #3 for which this ratio is 2.83 for the *CLS*). Then, despite the adopted selection criteria were only applied to the horizontal components of ground motions, compatibility of the selected records with amplitude and frequency content of the target motion can be thought of as fairly satisfied also for the vertical component of input motion.

Table 4 lists the main seismic parameters of the horizontal component of the scaled records: the mean and predominant periods T_m (Rathje et al., 1998) and T_p, the Arias intensity I_A (Arias, 1970), the destructiveness potential factor P_d (Araya and Saragoni, 1984) evaluated in the time-interval corresponding to the strong motion duration $D_{5\text{-}95}$ (Trifunac and Brady, 1975), and the equivalent number of loading cycles N_{eq} evaluated following Biondi et al. (2012); in Table 4 the peak value $(a_{v,g})_{scaled}$ of the vertical component of the scaled records and the corresponding scaling factor F_v are also listed.

Among the records selected for the *CLS*, records #1, #2 and #3 are characterised by values of T_m and T_p closer to the first natural period of elastic vibration of the dam T_{1e} and they are mostly rich in frequencies lower than f_{1e}, more relevant for the non-linear response of the dam; records #2 and #5 are instead characterised by the highest energy content, as it can be inferred by the large values of I_A, P_d and N_{eq}. For the *LLS*, records #3, #6 and #7 have mean and predominant periods closer to T_{1e}, while the highest values of I_A, P_d and N_{eq} characterise records #6 and #7. Thus, it can be anticipated that the major effects on the seismic response of San Pietro dam are induced by records #2 and #5 and by records #6 and #7 selected and properly scaled for the *CLS* and the *LLS*, respectively.

6. Numerical model and static analyses

The numerical analyses were carried out in terms of effective stresses using the finite difference code FLAC v.7.0 (ITASCA, 2011). Fig. 9 shows the grid adopted in the analyses: it consists of 13,845 quadrilateral zones and extends about three times the width of the embankment base, to ensure a negligible interaction of the dam with the vertical boundaries and to a depth of 25 m from the embankment base, including 18 m of the stiff formation.

In the static analyses, displacements were restrained in both directions at the bottom of the grid and horizontally at the side boundaries. The diaphragm, whose stiffness and strength do not affect the displacement analysis results, was modelled with a column of elements having the same stiffness of the adjacent soil but a permeability three orders of magnitude lower.

The dam and the foundation soils were described as elastic-perfectly plastic materials obeying the Mohr-Coulomb failure criterion; Table 5 lists the parameters assumed in the analyses as obtained from the geotechnical characterisation. The small-strain shear modulus G_0 was expressed as a function of the mean effective stress p' using the equation:

$$\frac{G_0}{p_r} = S \cdot \left(\frac{p'}{p_r}\right)^n R^m \tag{4}$$

where p_r = 100 kPa is a reference pressure, $R = p_y'/p'$ is the over-consolidation ratio expressed in terms of mean effective stress and S, n and m are non-dimensional stiffness coefficients. For the soils of the dam

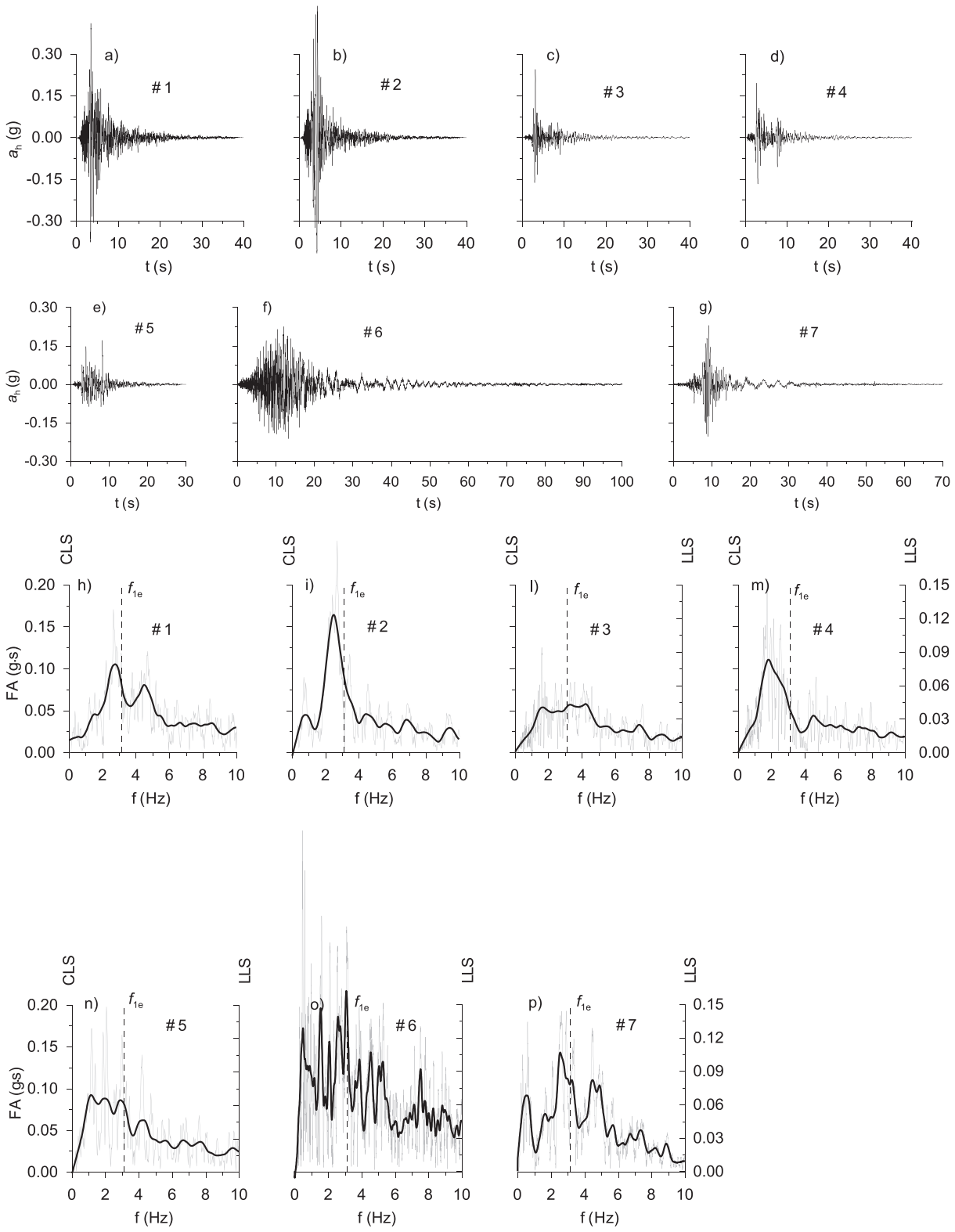

Fig. 6. Horizontal acceleration time histories (a-g) and corresponding Fourier amplitude spectra (h-p) of the selected seismic records.

it was assumed $R = 1$, while $n = 0.5$ was estimated as a function of *PI*. The stiffness multiplier S was evaluated by best fitting *CH* test results obtaining $S = 1860$ and $S = 5600$ for the fine-grained and the coarse-grained soils of the core and the shells, respectively. A constant shear modulus was assumed for the cemented alluvial layer, $G_0 = 0.56$ GPa, and the flysch formation, $G_0 = 1.1$ GPa. The profiles of small-strain shear modulus adopted in the analyses are in a fair agreement with the cross-hole test results of Fig. 3.

A hydrostatic pore water pressure was assumed in the foundation soil with water table at ground surface. The initial state of effective stress was computed simulating the staged construction of the dam, assumed as a drained process, and the subsequent impoundment. This is needed to evaluate the small-strain shear modulus distribution in the embankment at the end of dam construction. The operative shear stiffness

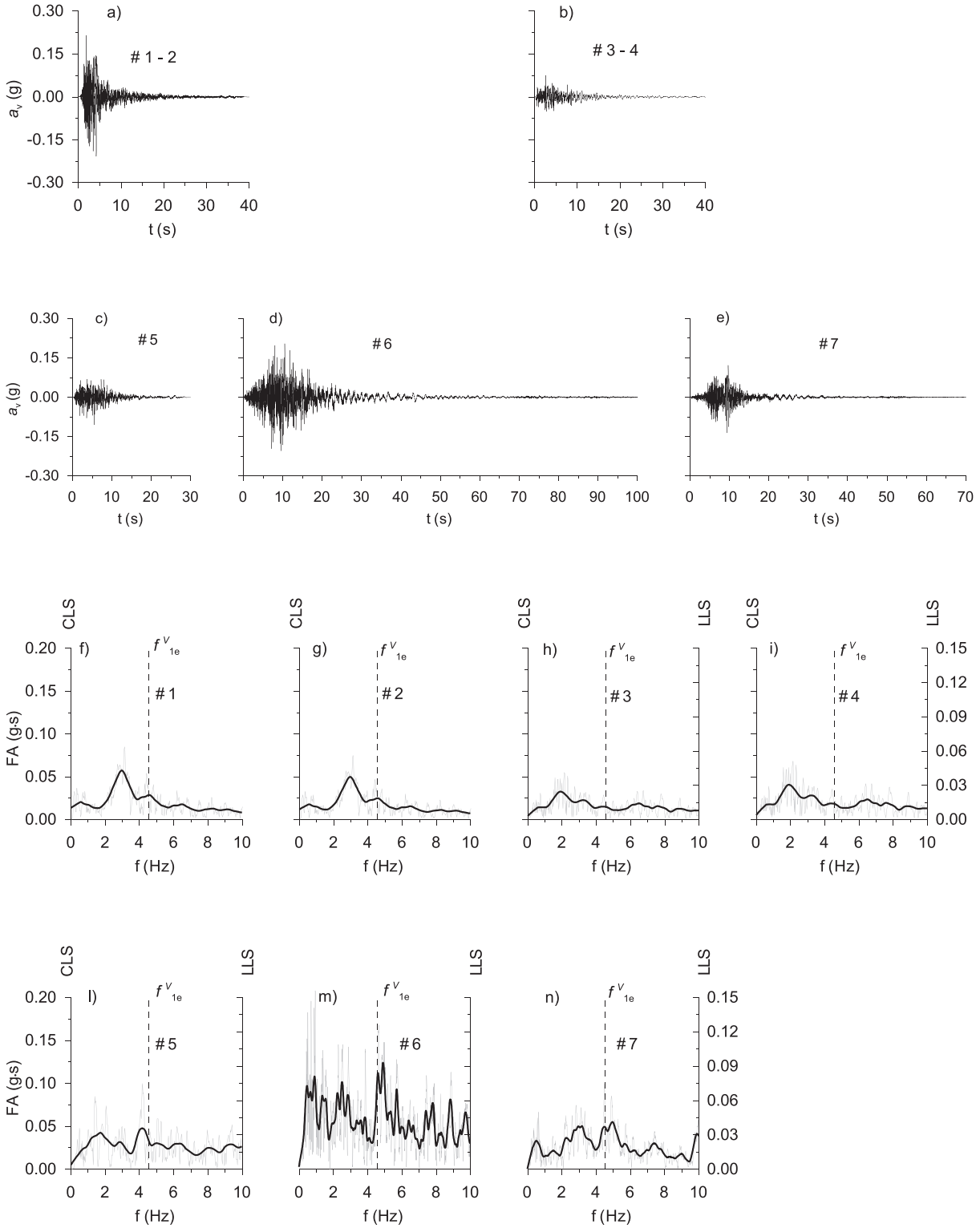

Fig. 7. Vertical acceleration time histories (a-e) and corresponding Fourier amplitude spectra (f-n) of the selected seismic records.

adopted in the static calculations were calibrated to reproduce the settlement profiles observed at the end of construction. At the end of each stage of dam construction, soil stiffness was updated according to Eq. (4) to be consistent with the new effective stress state. The settlement profiles measured by seven extensometers installed in the embankment, obtained following the procedure by Poulos et al. (1972) to isolate the dam deformation, are compared in Fig. 10 with those provided by the numerical analyses. On the average, a fair agreement is observed for the settlement profiles measured in the upstream slope (Fig. 10a), through the crest of the dam (Fig. 10b) and in the downstream slope (Fig. 10c).

After simulating the staged construction of the earth dam, a steady state seepage analysis was carried out. A hydrostatic water pressure was assumed acting upstream of the dam with $u = 0$ at the elevation of maximum storage level (464.8 m a.s.l) and zero pore water pressure was assigned at ground level, downstream of the dam, thus generating an unconfined seepage flow within the dam body. The seepage analyses

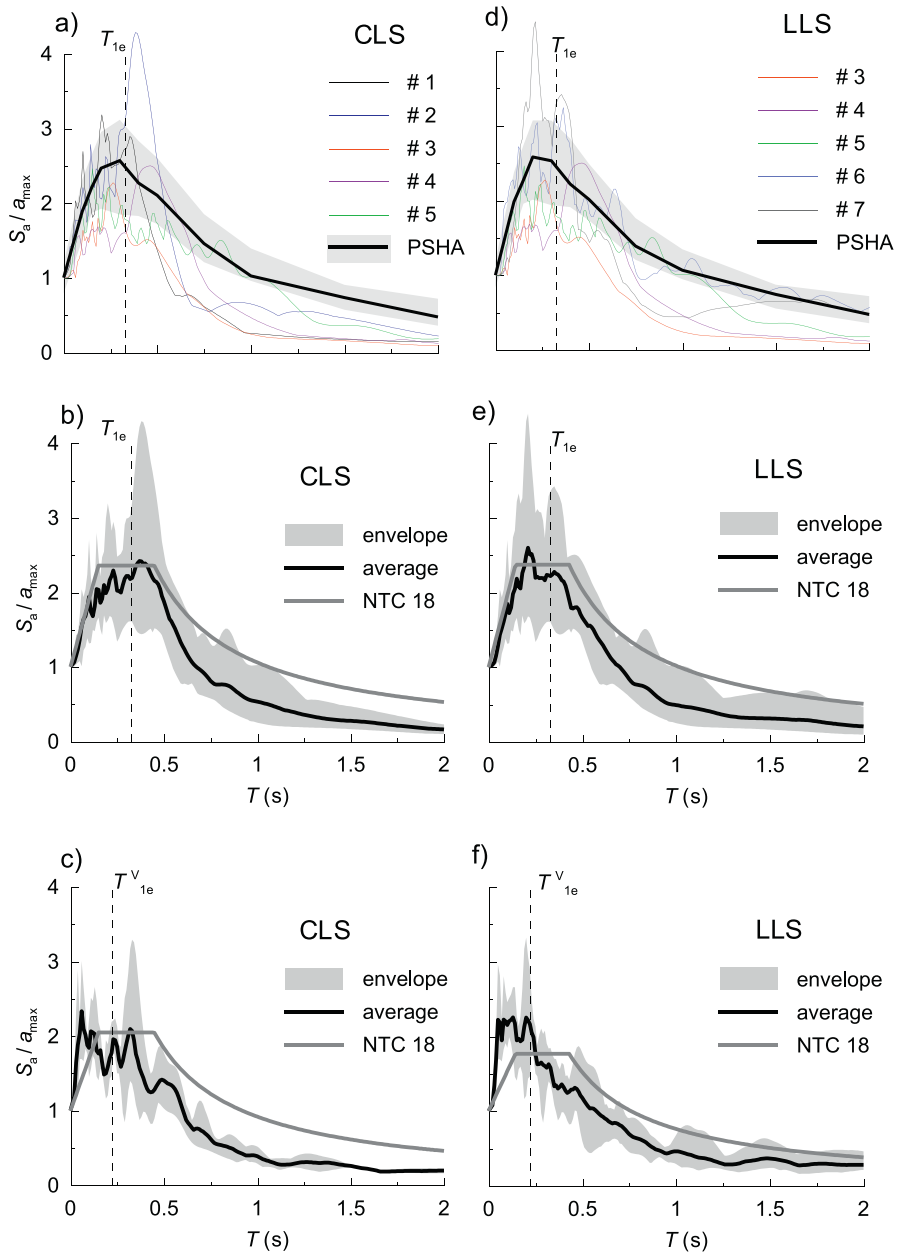

Fig. 8. Comparison between target spectral shape and normalised response spectra of the horizontal (a, b, d, e) and vertical (c, f) acceleration time histories selected for the CLS (a-c) and the LLS (d-f).

were carried out using the permeability coefficients listed in Table 5, back calculated to reproduce the hydraulic heads measured during operating conditions by the piezometers installed in the core (Calabresi et al., 2004).

Additional seepage analyses, carried out varying core permeability in the range of one order of magnitude, showed negligible changes of both phreatic surface and pore water pressure distribution in fact, for the specified range of permeability values, the core acts as an impervious material with respect to the coarse-grained material of the shells.

Fig. 11 shows the contour lines of total vertical stress σ_v, pore water pressure u, effective vertical stress σ'_v and mean effective stress p' in the dam and the foundation soils as obtained by the FD analyses. Owing to the presence of the reservoir, total vertical stresses are larger upstream (Fig. 11a). Pore water pressure is strongly affected by the low permeability of the core that results in an abrupt lowering of the water table downstream (Fig. 11b); maximum pore water pressure is about 500 kPa at the dam base. Due to the distribution of u, the contour lines of σ'_v and p' are bell-shaped, with larger values in the downstream portion of the dam (Fig. 11 c–d).

The static factor of safety computed, through the strength reduction technique implemented in the code FLAC, for steady state seepage conditions of the upstream and downstream slopes is equal to 1.89 and 1.69, respectively.

7. Screening-level seismic analyses

A series of screening-level analyses were performed for a preliminary assessment of the permanent deformations induced by earthquake loading and to identify the most critical seismic motions to input in the non-linear dynamic analyses. The screening-level analyses included finite differences (FD) pseudo-static analyses using the strength reduction technique, to detect the potential plastic mechanisms and the corresponding downhill critical acceleration $a_c = k_c \cdot g$ and one-way Newmark-type calculations, to evaluate permanent displacements

Table 4
Seismic parameters of the selected records scaled to the expected horizontal peak acceleration.

CLS: $(a_g)_t = 0.414$ *g*, $T_R = 1950$ years								
#	$(a_{v,g})_{scaled}$ (g)	$F_{s,v}$	T_p (s)	T_m (s)	I_A (m/s)	P_d (10^{-4} g·s^3)	$D_{5\text{-}95}$ (s)	N_{eq}
1	0.216	1.66	0.359	0.290	1.07	5.63	6.53	8.0
2	0.188	1.91	0.398	0.387	1.29	11.09	3.68	7.9
3	0.126	2.83	0.301	0.366	0.49	3.40	8.76	3.4
4	0.158	2.27	0.546	0.449	0.84	10.96	8.26	5.0
5	0.252	2.16	0.506	0.448	1.16	13.28	6.67	6.4

LLS: $(a_g)_t = 0.304$ *g*, $T_R = 949$ years								
#	$(a_{v,g})_{scaled}$ (g)	$F_{s,v}$	T_p (s)	T_m (s)	I_A (m/s)	P_d (10^{-4} g·s^3)	$D_{5\text{-}95}$ (s)	N_{eq}
3	0.093	2.43	0.301	0.366	0.26	1.83	8.76	3.4
4	0.116	1.95	0.546	0.449	0.45	5.91	8.78	5.0
5	0.185	1.85	0.506	0.448	0.63	7.16	6.67	6.4
6	0.276	0.82	0.323	0.517	2.38	16.01	19.65	39.1
7	0.179	1.26	0.392	0.500	0.84	14.82	9.20	9.0

induced by seismic loading. These latter were carried out by: *i*) double integration of the equation of relative motion (conventional one-way Newmark analysis); *ii*) through the application of the Makdisi and Seed (1978) procedure modified in the estimate of peak crest acceleration; *iii*) using available empirical relationships developed either assuming the soil mass to behave as a rigid body, or accounting for soil compliance via a decoupled or a coupled stick-slip analysis. Cyclic reduction of shear strength of dam and foundation soils was ignored or accounted for in a simplified way through a reduction of strength parameters.

7.1. Plastic mechanisms and corresponding critical acceleration

After simulating dam construction and the impoundment stage, pseudo-static analyses were performed by inclining gravity of an angle $\vartheta = tg^{-1}\,[k_h/(1\text{-}k_v)]$, k_h and k_v being the horizontal and vertical seismic coefficients. For each value of k_h the vertical seismic coefficient was assumed equal to either zero or $k_v = \pm\, 0.5{\cdot}k_h$ and the strength reduction technique implemented in FLAC was used to evaluate the safety factor *F*. The horizontal component $k_{h,c}$ of the critical seismic coefficient k_c corresponding to the condition $F = 1$ activates the critical plastic mechanism and represents a measure of the overall seismic resistance of the system (e.g. Masini et al., 2015).

To account for possible cyclic reduction of shearing resistance, the critical seismic coefficient was also evaluated using reduced values of strength parameters. Specifically, following Makdisi and Seed (1978) a 20% reduction of the shear strength was considered for the coarse-grained soil of the shells introducing a reduced angle of shearing resistance $\tan\varphi'^* = 0.8{\cdot}\tan\varphi'$ (Table 5), this leading to a reduced value of the critical seismic coefficient $k_{h,c}$.

Fig. 12 shows the contours of shear strain rate computed in critical conditions ($k_h = k_{h,c}$), assuming $k_v = -\,0{,}5k_h$ (inertia forces directed upwards), ignoring (Fig. 12a) or accounting (Fig. 12b) for the strength reduction. In both cases, a plastic mechanism on the upstream side is activated, that is shallow, of low curvature, with shear strains occurring in narrow bands, not affecting the core of the dam. Dam capability to retain the water reservoir is then maintained for the considered seismic scenario, rehabilitation works being needed at the end of the earthquake. The mechanism computed ignoring the cyclic strength reduction extends to a depth y_f from the crest of the dam equal to about 70% of its height $H_d = 48$ m (Fig. 12a), while $y_f = 0.5{\cdot}H_d$ is obtained if a reduction of shear strength is considered in the analyses (Fig. 12b).

Assuming $k_v = -\,0.5{\cdot}k_h$ a critical seismic coefficient $k_{h,c} = 0.176$ is computed for the upstream side, that reduces to $k_{h,c}^* = 0.131$ when accounting for the reduction of shear strength. Since for $k_v = 0$ it is $k_{h,c} = 0.190$ and $k_{h,c}^* = 0.140$, the influence of the vertical component of the inertial forces is not crucial in that ignoring k_v results in increments of only about 6–7% in the values of $k_{h,c}$ and $k_{h,c}^*$. According to the computed plastic mechanisms, the scheme of infinite slope can be thought of as an appropriate simplified scheme for a preliminary

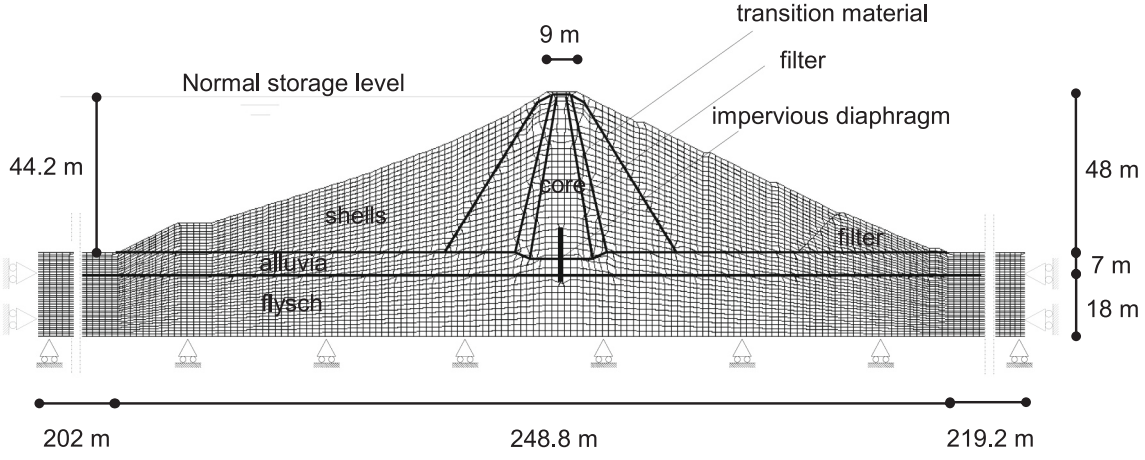

Fig. 9. Finite difference grid adopted in the static and pseudo-static analyses.

Table 5
Mechanical parameters adopted in the numerical analyses.

	Bedrock	Alluvia	Shells	Transition material	Filters	Core	Filter (downstream)
γ [kN/m^3]	23	23	23	19.9	19.9	19.9	23
c' [kPa]	1	1	1	30	30	30	1
φ' (φ'*) [°]	42 (36)	42 (36)	36 (30)	26	26	26	36
k [m/s]	$1.5{\cdot}10^{-8}$	$1.0{\cdot}10^{-6}$	$1.0{\cdot}10^{-6}$	$1.0{\cdot}10^{-6}$	$1.8{\cdot}10^{-7}$	$1.5{\cdot}10^{-8}$	$1.0{\cdot}10^{-6}$

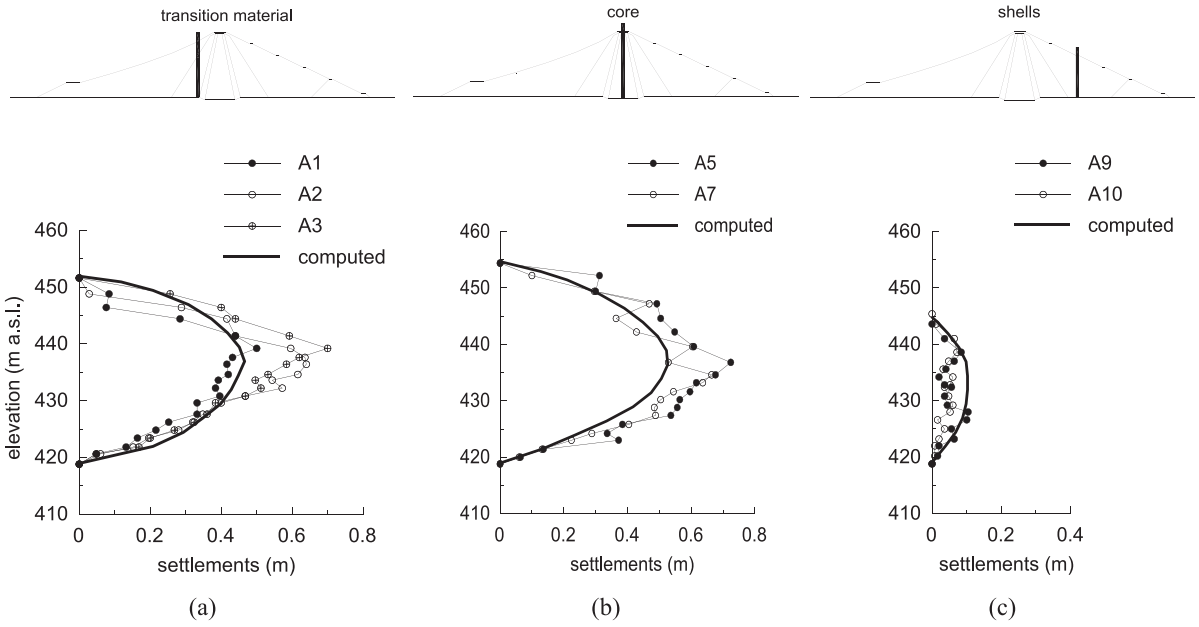

Fig. 10. Observed and computed settlement profiles during dam construction.

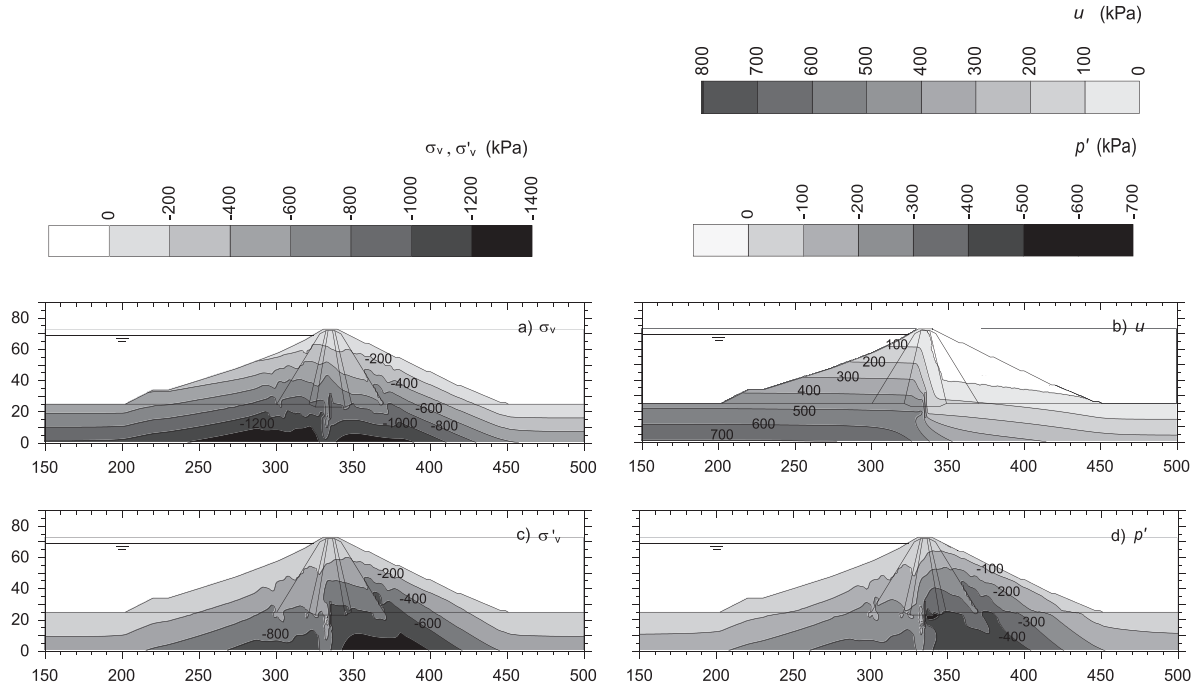

Fig. 11. Contours of total vertical stress (a), pore water pressure (b), effective vertical stress (c) mean effective stress (d). Negative stresses mean compression.

evaluation of the permanent displacements induced by earthquake loading.

7.2. Newmark-type analyses

Newmark-type analyses were carried out assuming one-way translational sliding of a rigid block. For the scheme of infinite slope, the ground surface and the sliding surface are inclined of an angle α to the horizontal and the equation of relative motion is written in the form:

$$\ddot{d} = \frac{cos(\varphi' - \alpha)}{cos\varphi'}\ddot{d}_0 \tag{5}$$

where $\ddot{d}$ and $\ddot{d}_0$ are the relative acceleration of a block sliding along a plane of inclination α and a horizontal plane, respectively, and φ' is the angle of shearing resistance along the sliding surface. Since the shape factor:

$$S = \frac{cos(\varphi' - \alpha)}{cos\varphi'} \tag{6}$$

is constant, the permanent displacement d of the block sliding along the failure plane is computed as:

$$d = S \cdot d_0 \tag{7}$$

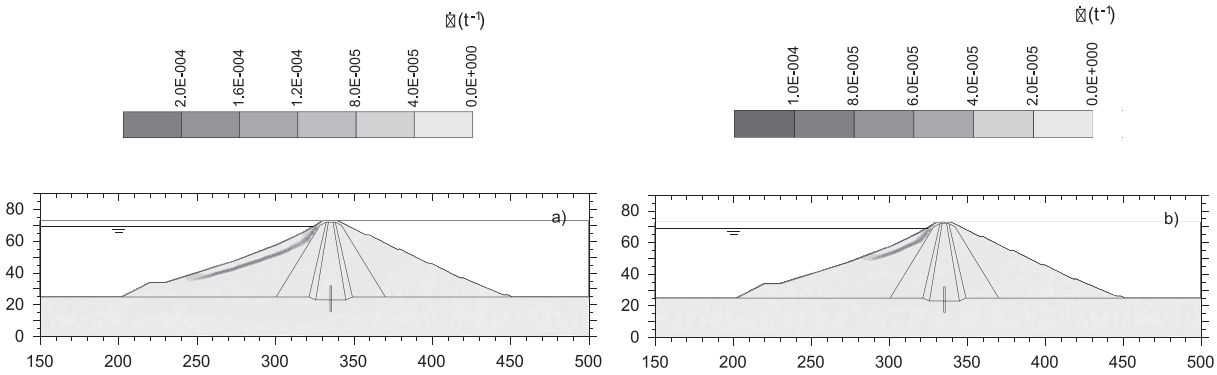

Fig. 12. Contours of shear strain rate at critical conditions ($k_h = k_{h,c}$) for full (a) and reduced (b) shear strength.

d_o being the permanent displacement computed for the one-way sliding along a horizontal plane.

The contour lines of Fig. 12 suggest $\alpha \approx 27°$, with values of $\varphi' = 36°$ and $\varphi'^* = 30°$ adopted when ignoring or considering shear strength reduction (Table 5). The horizontal ($d_h = d{\cdot}\cos\alpha$) and vertical ($d_v = d{\cdot}\sin\alpha$) components of d were evaluated assuming the crest settlement u_c be equal to the maximum vertical displacement $d_{v,max}$.

Despite the well-known coupling between the stratigraphic and the topographic amplification effects (e.g. Rizzitano et al., 2014; Papadimitriou, 2019), a simplified evaluation of ground motion amplification in the embankment was obtained scaling the horizontal component of the acceleration time histories by the topographic (S_T) and the stratigraphic (S_S) amplification factors, as prescribed by the NTC18 (2018) that adopts the same rules of Annex A of Eurocode 8-5 (Eurocode 8-5, 2003).

A value of the topographic factor $S_T = 1.2$ was adopted with reference to the slope of the shells only, as prescribed for ridges with crest width significantly less than the base width and slope angles less than 30°.

The stratigraphic factor S_s is instead provided as a function of the soil class, the target acceleration a_g and the amplification factor F_o of the maximum spectral acceleration, the two latter being site dependent parameters. For the case at hand, the soil class was defined by the equivalent shear wave velocity $V_{S,H}$ computed in the upper 30 m of the dam body. To this purpose the average small-strain shear modulus ($G_{0,ave}$) and soil density ($\rho_{,ave}$) profiles needed to evaluate the profile of $V_S = (G_{0,ave}/\rho_{ave})^{0.5}$ were obtained weighting the values of G_0 and ρ of the i^{th} row of the model grid adopted in the *FD* analyses by the element width. An equivalent shear wave velocity $V_{S,H} = 353$ m/s was obtained, this corresponding to a soil of class *C* (medium-dense coarse-grained soil or medium stiff fine-grained soil) with 180 m/s $< V_{S,H} <$ 360 m/s for which it is $1 \le S_s = 1{,}7\text{-}0{,}6{\cdot}F_o\,a_g/g \le 1.5$. Accordingly, values of $S_S = 1.268$ and 1.114 were computed for the *LLS* ($F_o = 2.371$, $a_g = 0.304\,g$) and the *CLS* ($F_o = 2.357$, $a_g = 0.414\,g$), respectively.

For each of the selected seismic records both signs of the selected acceleration time histories were considered with d_0 denoting the maximum of the two computed displacements. The results of the Newmark computations are shown with a full circle in Figs. 13–14 in terms of horizontal (d_h) and vertical (d_v) permanent displacements, computed ignoring (Fig. 13) or accounting (Fig. 14) for possible shear strength reduction.

Irrespective of strength reduction and the limit state, the horizontal and vertical displacements are generally $d_h \le 0.16$ m and $u_c = d_{v,max} \le 0.06$ m, with the only exception of those evaluated using record #6 for which the displacements induced by seismic shaking are about 1.5 times higher ($d_{h,max} = 0.22$ m and $u_c = d_{v,max} = 0.09$ m).

It is worth noting that, since it is $a_g{\cdot}S_S{\cdot}S_T = 0.140\,g$ and $0.182\,g$ for the *OLS* ($F_o = 2.501$, $a_g = 0.078\,g$, $S_S = 1.5$) and the *DLS* ($F_o = 2.494$, $a_g = 0.101\,g$, $S_S = 1.5$), respectively, and in the worst case ($k_v = -0.5{\cdot}k_h$) it is $k_{h,c} = 0.176$ and $k_{h,c}^* = 0.131$, negligible displacement (less than 7 mm) were computed for the serviceability limit states.

7.3. Modified Makdisi & Seed procedure

In the Makdisi and Seed (1978) procedure the dynamic response of the dam is taken into account through an acceleration coefficient β defined as the ratio between the maximum value of an equivalent acceleration acting in the sliding mass, $a_{h,ave}$, and the peak acceleration $a_{max,crest}$ at the crest of the dam.

The displacement calculation is accomplished by two charts providing β as a function of the normalised depth of the toe of the failure surface (z_y/H_d), while the normalised displacement $d^*(= d/[a_{h,ave}{\cdot}T])$ is a function of the critical acceleration ratio $a_{h,c}/a_{h,ave}$ and earthquake magnitude M.

The reliability of this procedure depends on the evaluation of the peak acceleration at the crest of the dam $a_{max,crest}$ that is affected by a number of uncertainties.

Originally, $a_{max,crest}$ was evaluated through an iterative procedure, modelling the dynamic response of the embankment as a Bessel-series approximation with strain-dependent elastic properties. However, non-linear dynamic response of the dam and the foundation soils, together with possible frequency coupling, can lead to crest accelerations larger than those predicted by this procedure. Moreover, any dynamic analysis of higher complexity, for an accurate estimate of $a_{max,crest}$, conflicts with the intent of a simplified method (Bray, 2007).

Accordingly, the procedure proposed by Papadimitriou et al. (2014) was adopted herein to evaluate $a_{max,crest}$, since it accounts in a simple way for the effects of non-linear soil behaviour and possible coupling between non-linear period of dam (T_1) and foundation (T_b) soils and the frequency content of the selected input motion, represented by its predominant period T_p. Also, $T = T_1$ was assumed to estimate the permanent displacement d starting from the normalised values d^* defined by Makdisi and Seed (1978).

For each of the input motions selected for the two limit states, the modified procedure was applied to the potential failure mechanism detected in the upstream shell of the dam. Specifically: the maximum free-field $a_{max,ff}$ and crest $a_{max,crest}$ accelerations, as well as the period of the foundation soil T_b and its elastic value T_{be}, were related to the layer of alluvial gravels ($H_b = 7$ m, $V_b = 489$ m/s); earthquake magnitudes $M = 6.5$ and $M = 7.5$ were assumed for the *LLS* and the *CLS*, respectively; for a safe estimate and to account for the variability of the acceleration coefficient β given by the Makdisi & Seed charts, maximum values of coefficient β were considered for each failure mechanism to compute $a_{h,ave}$.

Table 6 lists the values of computed peak crest acceleration $a_{max,crest}$ together with the variables relevant to the procedure by Papadimitriou et al. (2014). As an example, for the record *#1* selected for the *CLS* ($a_g =$

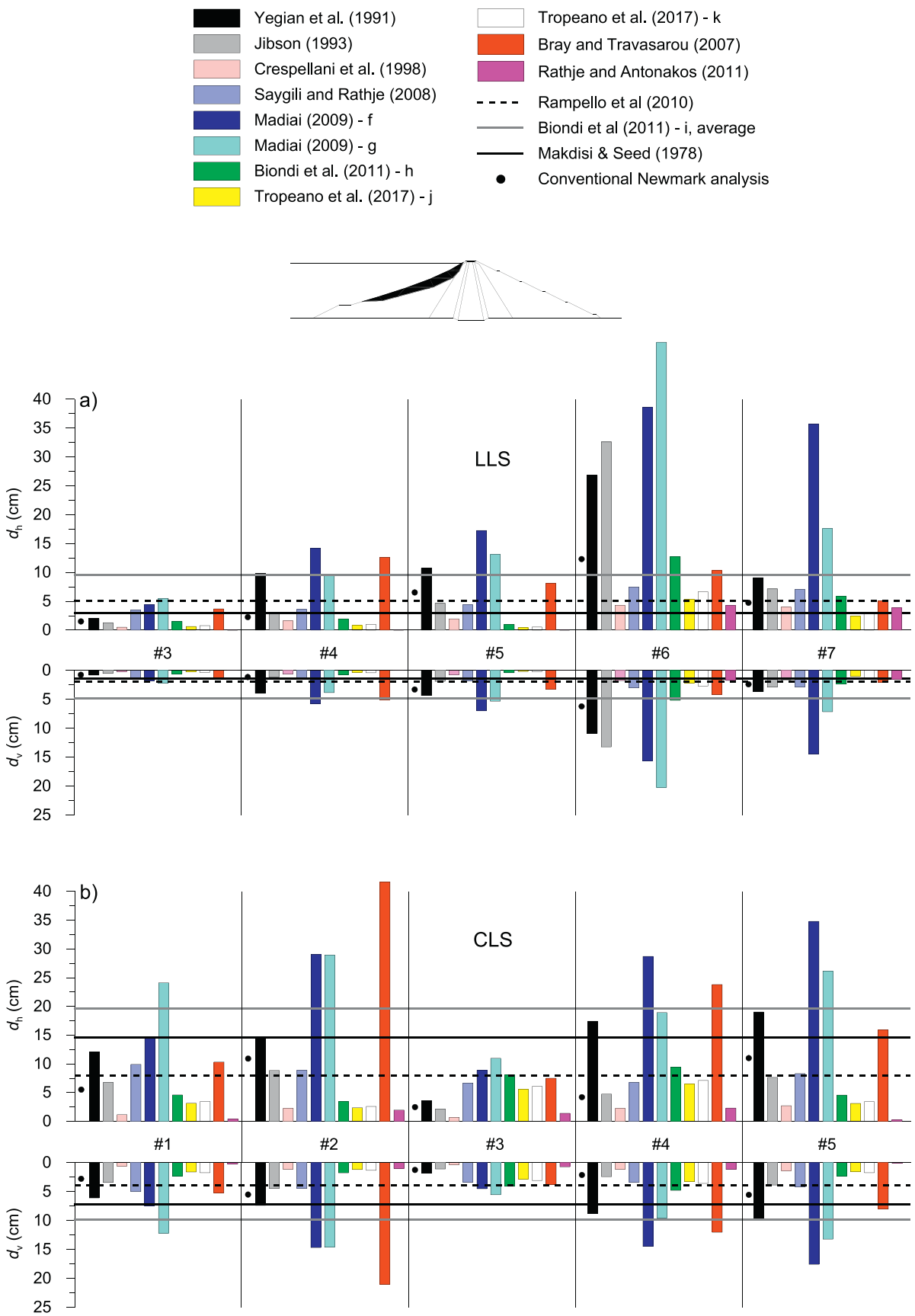

Fig. 13. Horizontal (d_h) and vertical (d_v) permanent displacements computed for the upstream slope with reference to the *LLS* (a) and the *CLS* (b), ignoring possible reduction of shear strength.

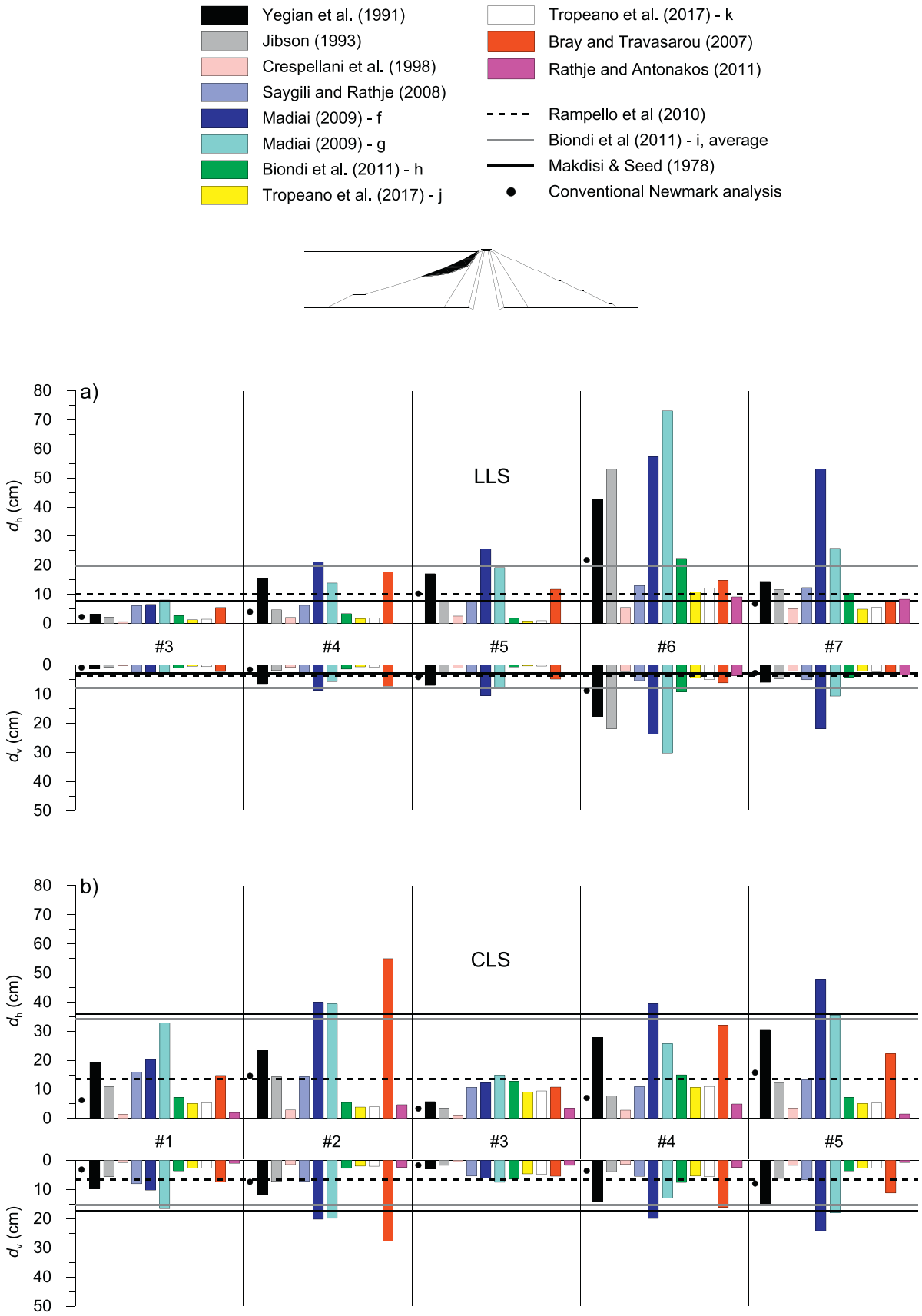

Fig. 14. Horizontal (d_h) and vertical (d_v) permanent displacements computed for the upstream slope with reference to the *LLS* (a) and the *CLS* (b), accounting for the soil shear strength reduction.

Table 6
Horizontal and vertical permanent displacements computed through the combined Makdisi and Seed (1978) and Papadimitriou et al. (2014) procedures.

	CLS ($T_b/T_{be} = 1.30$)					*LLS* ($T_b/T_{be} = 1.22$)				
record	#1	#2	#3	#4	#5	#3	#4	#5	#6	#7
T_b / T_p	0.21	0.19	0.25	0.14	0.15	0.23	0.13	0.14	0.22	0.18
$a_{max,ff}$ (g)	0.433	0.430	0.441	0.422	0.424	0.323	0.310	0.311	0.320	0.315
T_1 / T_{1e}	0.891	0.804	1.063	0.586	0.632	1.063	0.586	0.632	0.991	0.816
$a_{max,crest}$ (g)	0.751	0.781	0.703	0.786	0.788	0.550	0.576	0.578	0.565	0.586

strength reduction	Limit state	*M*	d_h (cm)	d_v (cm)
No	*CLS*	7.5	7.9-14.5	4.0-7.3
	LLS	6.5	1.0-2.9	0.5-1.5
Yes	*CLS*	7.5	19.5-35.7	9.8-17.6
	LLS	6.5	3.0-7.5	1.5-3.8

0.414 *g*, $T_p = 0.359$ s), according to Papadimitriou et al. (2014) it is $T_{be} = 4{\cdot}H_b/V_b = 0.057$ s and $T_b/T_{be} = 1.30$, this leading to a non-linear period of the foundation soils equal to $T_b = 0.074$ s. Also, since it is $T_b/T_p = 0.21$ and $T_{1e}/T_p = 0.891$, the amplification ratio due to the foundation soils is $a_{max,ff}/a_g = 1.046$ (providing a maximum free-field acceleration $a_{max,ff} = 0.433$ *g*) and $T_1/T_{1e} = 1.861$. Thus, the non-linear period of vibration of the dam is $T_1 = 0.596$ s (with $T_1/T_p = 1.659$) and the dam amplification ratio is $a_{max,crest}/a_{max,ff} = 1.734$, leading to a peak crest acceleration equal to $a_{max,crest} = 0.751$ *g*.

The same procedure was applied to all the selected ground motions obtaining peak horizontal crest acceleration $a_{max,crest}$ in the range 0.703 *g* - 0.788 *g* and 0.550 *g* - 0.586 *g* for the *CLS* and the *LLS*, respectively (Table 6). Herein, the maximum values $a_{max,crest} = 0.788$ *g* (*CLS*, record #5) and $a_{max,crest} = 0.586$ *g* (*LLS*, record #7) were considered for a safe estimate of permanent displacements.

For the mechanism detected in the upstream shell in the analyses which account for the strength reduction ($a_{h,c} = 0.131$ *g*, $y_f/H_d \approx 0.5$) and with reference to the record *#1* selected for the *CLS*, the Makdisi & Seed charts provide a maximum value of the acceleration coefficient $\beta_{max} = a_{h,ave}/a_{max,crest} \approx 0.740$ ($a_{h,ave} = 0.579$ *g*) and, since $a_{h,c}/a_{h,ave} = 0.226$, a normalised displacement d^* ranging from about 0.12 to about 0.21, leading to a peak value of the permanent displacement $d = 0.39$ m with horizontal and vertical components equal to $d_h = 0.35$ m and $d_v = 0.18$ m, respectively.

The ranges of d_h and d_v computed for the whole sets of seismic records selected for the two selected limit states (*LLS* and *CLS*) ignoring or accounting for the strength reduction are given in Table 6 while maximum computed values of d_h and d_v are plotted in Figs. 13–14 by a black solid line.

For the *LLS*, permanent displacement d_h increases from 0.03 to 0.075 m when accounting for shear strength reduction, with a crest settlement $u_c = d_{v,max} = 0.038$ m (Fig. 14a); depending on the considered input motion, these values are larger or smaller than those provided by the conventional Newmark-type analysis: $d_h = 0.02 \div 0.22$ m and $u_c = d_{v,max} = 0.01 \div 0.09$ m (Fig. 14a).

Conversely, for the *CLS* (Figs. 13b, 14b) the horizontal and vertical permanent displacements computed through the modified Makdisi & Seed procedure proposed herein are $d_h = 0.145$ m and $d_v = 0.073$ m ignoring shear strength reduction, while, it is $d_h = 0.357$ m and $d_v = 0.176$ m accounting for it. A 20% reduction of the shear resistance then results in an earthquake induced displacement about 2.5 times higher. In this case, regardless the considered input motion, the conventional Newmark-type analysis leads to smaller permanent displacements with crest settlements $u_c = d_{v,max}$ always lower than about 0.08 m (Fig. 14b).

7.4. Empirical relationships

Evaluation of permanent displacements was also performed using thirteen empirical relationships proposed in the literature (Table 7); they were derived by different sets of seismic records fitting the results of Newmark-type computations. Some of them (Yegian et al., 1991; Jibson, 1993; Crespellani et al., 1998; Rampello et al., 2010; Saygili and Rathje, 2008; Madiai, 2009; Biondi et al., 2011) can be considered as appropriate for shallow and stiff landslides, while the others (Tropeano et al., 2017; Rathje and Antonakos, 2011) account for soil compliance via the decoupled approach in which the seismic motion is first evaluated through one- or two-dimensional ground response analyses, and the earthquake-induced displacements are then computed through a conventional sliding-block analysis. The relationships by Bray and Travasarou (2007) were also used, that are based on a coupled stick-slip analysis and account for soil compliance and non-linear soil behaviour. Some of the selected relationships have been widely used in the literature for a preliminary assessment of the seismic performance of dams (e.g. Vecchietti et al., 2019) though in some cases underestimate actual displacements observed in documented case-histories (Meehan and Vahedifard, 2013).

Table 7 provides the standard deviation of the corresponding regression model and the relevant symbols and notations. In the analyses:

- the selected ground motions were amplified using stratigraphic and topographic amplification factors S_S and S_T for relationships (*a*) to (*i*), while only S_T was considered for relationships (*j*) to (*m*), that inherently account for stratigraphic amplification;
- the seismic parameters needed in the relationships were computed using the acceleration time-histories of the selected input motions;
- starting from the results of the probabilistic seismic hazard analysis (NTC18, 2018) and for the considered soil class *C*, the period corresponding to the end of the constant spectral acceleration branch was assumed $T_c = 0.614$ and 0.596 for *CLS* and *LLS*;
- the predominant period T_p was deduced from the smoothed Fourier spectra (Fig. 8, Table 4);
- the fundamental period T_s was assumed equal to $T_1 = 0.32$ s (Cascone et al., 2021);
- values of parameters $A = 7.40$, $B_2 = 0.75$ m and $A_{2a} = -3.537$, $B_{2a} = -1.269$, needed in the relationships proposed by Rampello et al. (2010) and Biondi et al. (2011) were assumed for both the *CLS* and *LLS* assuming a soil class *C* and $a_g > 0.35$ *g*.

The mean horizontal (d_h) and vertical (d_v) displacements computed using the selected relationships are plotted in Figs. 13 and 14. Some of them provide displacements greater than those evaluated by the Newmark analysis and the modified Makdisi and Seed (1978) procedure. As an example, for the record #1 selected for the CLS and for the analyses which account for the strength reduction (Fig. 14), the empirical relationships provide values of d_h and d_v up to 0.33 m and 0.17 m, respectively. Conversely displacement components $d_h = 0.02 \div 0.22$ m and $d_v = 0.01 \div 0.09$ m are evaluated using the conventional Newmark-type analysis (§ 7.2) and $d_h = 0.35$ m with $d_v = 0.18$ m are obtained through the modified Makdisi and Seed (1978) procedure (§ 7.3).

Table 7
Empirical relationships adopted to evaluate earthquake-induced displacements.

	Reference		Proposed relationship	Note
Rigid soil mass	*a*	Yegian et al. (1991)	$log\overline{d_0} = log\left(\frac{d_0}{N_{eq}\cdot a_{h,max}\cdot T_p^2}\right) = 0.22 - 10.12\cdot\left(\frac{k_{h,c}}{k_{h,max}}\right) + 16.38\cdot\left(\frac{k_{h,c}}{k_{h,max}}\right)^2 - 11.48\cdot\left(\frac{k_{h,c}}{k_{h,max}}\right)^3$	$\sigma_{log\overline{d_0}} = 0.45$
	b	Jibson (1993)	$\log d_0 = 1.460\cdot\ \log I_A - 6.642\cdot k_{h,c} + 1.546$	$\sigma_{\log d_0} = 0.409$
	c	Crespellani et al. (1998)	$d_0 = 0.108\cdot P_d^{0.977}\cdot k_{h,c}^{-1.023}$	upper bound (90% confidence level)
	d	Rampello et al. (2010)	$d_0 = B_2\cdot e^{-A\cdot\frac{k_{h,c}}{k_{h,max}}}$	upper bound (94% confidence level)
	e	Saygili and Rathje (2008)	$lnd_0 = -1.56 - 4.58\cdot\left(\frac{k_{h,c}}{k_{h,max}}\right) - 20.84\cdot\left(\frac{k_{h,c}}{k_{h,max}}\right)^2 + 44.75\cdot\left(\frac{k_{h,c}}{k_{h,max}}\right)^3 + -30.50\cdot\left(\frac{k_{h,c}}{k_{h,max}}\right)^4 - 0.64\cdot ln(a_{h,max}) + 1.55\cdot ln(v_{h,max})$	$\sigma_{lnd_0} = 0.41 + 0.52\cdot\frac{k_{h,c}}{k_{h,max}}$
	f	Madiai (2009)	$d_0 = 1.90\cdot r\cdot P_d\cdot\left(1-\frac{k_{h,c}}{k_{h,max}}\right)^{2.72}\cdot\left(\frac{k_{h,c}}{k_{h,max}}\right)^{-0.60}$	$r = 1.0$: mean (50%) $r = 2.9$: upper-bound (90%)
	g	Madiai (2009)	$d_0 = 0.156\cdot r\cdot I_A\cdot\left(1-\frac{k_{h,c}}{k_{h,max}}\right)^{2.60}\cdot\left(\frac{k_{h,c}}{k_{h,max}}\right)^{-0.60}$	$r = 1.0$: mean (50%) $r = 3.0$: upper-bound (90%)
	h	Biondi et al. (2011)	$log\overline{d_0} = log\left(\frac{d_0}{a_{h,max}\cdot T_m\cdot D_{5-95}}\right) = A_{2a}\cdot\left(\frac{k_{h,c}}{k_{h,max}}\right) + B_{2a}$	$\sigma_{log\overline{d_0}} = 0.276$
	i	Biondi et al. (2011)	$log\overline{d_0} = log\left(\frac{d_0}{a_{h,max}\cdot g\cdot 19.914\cdot T_c^{1.854}}\right) = A_{2a}\cdot\left(\frac{k_{h,c}}{k_{h,max}}\right) + B_{2a}$	$\sigma_{log\overline{d_0}} = 0.276$
Compliant soil mass	*j*	Tropeano et al. (2017)	$log\overline{d_0} = log\left(\frac{d_0}{a_{h,max}\cdot T_m\cdot D_{5-95}}\right) = -1.349 - 3.410\cdot\frac{k_{h,c}}{k_{h,max}}$	$\sigma_{log\overline{d_0}} = 0.35$
	k	Tropeano et al. (2017)	$log\overline{d_0} = log\left(\frac{d_0}{a_{h,max}\cdot T_m\cdot D_{5-95}}\right) = -2.571 + 2.389\cdot log\left(1-\frac{k_{h,c}}{k_{h,max}}\right) - 1.125\cdot log\left(\frac{k_{h,c}}{k_{h,max}}\right)$	$\sigma_{log\overline{d_0}} = 0.35$
	l	Bray and Travasarou (2007)	$lnd_0 = -1.10 - 2.83\cdot lnk_{h,c} - 0.333\cdot(lnk_{h,c})^2 + 0.566\cdot lnk_{h,c}\cdot lnS_a + +3.04\cdot lnS_a - 0.244\cdot(lnS_a)^2 + 1.50\cdot T_s + .0.278\cdot(M_w - 7)$ if $T_s > 0.05s$ $lnd_0 = -0.22 - 2.83\cdot lnk_{h,c} - 0.333\cdot(lnk_{h,c})^2 + 0.566\cdot lnk_{h,c}\cdot lna_{h,max} + +3.04\cdot lna_{h,max} - 0.244(lna_{h,max})^2 + 0.278\cdot(M_w - 7)$ if $T_s < 0.05s$	$\sigma_{lnd_0} = 0.67$ $S_a = S_a(1.5\cdot T_s)$
	m	Rathje and Antonakos (2011)	$lnd_0 = lnd_{0(eq.e)} + 1.42\cdot T_s$ if $T_s \le 0.5$ $d_{0(eq.e)} = d_0$ by equation (e) $lnd_0 = lnd_{0(eq.e)} + 0.71\cdot T_s$ if $T_s > 0.5$	$\sigma_{lnd_0} = 0.40 + 0284\cdot\frac{k_{h,c}}{k_{h,max}}$

$a_{h,c} = k_{h,c}\cdot g$: horizontal component of the yield acceleration
$a_{h,max} = k_{h,max}\cdot g$, $v_{h,max}$: peak horizontal acceleration and velocity
T_p: predominant period
T_m: mean period
T_c: period evaluated according to NTC18 (2018)
T_s: fundamental period of the sliding mass
$S_a(T)$: spectral ordinate of the selected record
$D_{5\text{-}95}$: strong motion duration
I_A: Arias Intensity
P_d: destructiveness potential factor
N_{eq}: number of equivalent loading cycles
M_w: moment magnitude
A, B_2: regression coefficients
A_{2a}, B_{2a}: regression coefficients

In the analyses carried out for the *LLS* ignoring the shear strength reduction (Fig. 13a), d_h and d_v are generally lower than about 0.17 m and 0.07 m (#5), with the only exception of records #6 and #7 for which d_h increases to 0.36 m (#7) and 0.50 m (#6) with the largest crest settlement $u_c = d_{v,max} = 0.20$ m (#6).

Records #6 and #7 are still the most severe when accounting for reduction of shear strength (Fig. 14a), with horizontal displacement increasing to about $d_h = 0.73$ m and the maximum crest settlement $u_c = 0.30$ m. Irrespective of possible reduction of shear strength, for all the *LLS* records the highest permanent displacements are computed by the relationship proposed by Madiai (2009) that uses the Arias intensity I_A and the destructiveness potential factor P_D. Then, the larger displacements obtained from records #6 and #7 can be ascribed to their high energy content in addition to their long duration $D_{5\text{-}95}$ and large number of equivalent loading cycles N_{eq} (Table 7). This is consistent with the results of Pagano and Sica (2013) which identified the Arias intensity as a proper parameter to be used as a cause variable in arranging cause-effect relationships for dams subjected to large earthquakes.

Possible coupling between the vibration frequencies of the dam ($T_s = T_{1e} \approx 0.3$ s) and the frequency content of ground motions #3, #6 and #7, ($T_p \approx 0.3$–0.4 s), cannot be appreciated by a sliding analysis of a rigid block so that the large displacements computed using the relationships by Yegian et al. (1991) and Jibson (1993) can only be ascribed to the high values of N_{eq} and I_A of record #6 (Table 4). On the whole, in the worst case (#6), the highest crest settlement computed for the *LLS* is $u_c = 0.30$ m, that is substantially lower than the dam freeboard (2.0 m). Moreover, the corresponding normalised crest settlement $u_c/H = 0.54\%$ is lower than the threshold value of 1.25% associated to possible occurrence of a *LLS* (Aliberti et al., 2019).

Greater permanent displacements have been generally computed for the *CLS* both ignoring (Fig. 13b) or accounting (Fig. 14b) for possible shear strength reduction. In the first case (Fig. 13b), the vertical and horizontal permanent displacements are generally lower than about 0.18 and 0.35 m, respectively, with the only exception of those computed using record #2. Depending on the empirical relationships, the higher value of d_h is in the range of 0.26 to 0.42 m, while $d_v = 0.13$–0.21 m, records #2 and #5 being the most critical. When accounting for earthquake-induced strength reduction (Fig. 14b), the largest displacements are obtained using the relationship by Bray and Travasarou (2007) with record #2: $d_h = 0.55$ m and $d_v = 0.28$ m.

This result cannot be attributed to dynamic coupling between the vibration period of the dam ($T_s = T_{1e} \approx 0.3$ s) and the predominant or mean period of record #2 ($T_p \approx T_m \approx 0.4$ s) in that similar periods ($T_p \approx 0.30$–0.36 s, $T_m \approx 0.29$–0.37 s) also characterise records #1 and #3 that, however, provided significantly lower displacements ($d_h = 0.15$–0.33 m, $d_v = 0.07$–0.17 m, Fig. 14b). Conversely, it can be ascribed to the moment magnitude ($M_w = 6.9$) of the corresponding seismic event, whose effect is explicitly accounted for in the relationship by Bray and Travasarou (2007).

For all the remaining records, the larger permanent displacements are provided by the relationship proposed by Madiai (2009) with higher values computed using records #2, #4 and #5 characterised by the higher Arias intensity I_A and destructiveness potential P_d (Table 4). For the *CLS* also, the largest crest settlement induced by earthquake loading ($u_c = 0.28$ m) is much lower than the freeboard of the dam and is lower than the threshold value of 1.0 m which was associated to a *major damage* by Seed (1979) and Hynes-Griffin and Franklin (1984). The corresponding normalised crest settlement, $u_c/H = 0.51\%$, is lower than the threshold value 2.5% associated to the achievement of a *CLS* (Aliberti et al., 2019).

8. Concluding remarks

Many large dams were designed before the establishment of a seismic code, so that the assessment of their seismic performance and the maintenance of post-seismic operational conditions is an important issue. In this paper, the seismic performance of the San Pietro dam has been evaluated using conventional methods of analysis with reference to the possible occurrence of a Life Safety or a Collapse Limit State. Specifically, the paper describes the procedure adopted to select two sets of input ground motions for each ultimate limit state and the results of screening-level seismic analyses based on a numerical model of the dam calibrated against the settlements of the dam monitored during construction.

The input motions were defined in terms of acceleration time-histories using a compatibility criterion to match the amplitude and the frequency content of proper target motions in an interval of vibration periods relevant for the non-linear response of the dam. These, in turn, were defined through a close scrutiny of the data derived from historical seismicity at the dam site and a review of the most recent probabilistic seismic hazard analysis available for the same site. For each of the limit state to be checked, proper performance indexes were considered in terms of threshold values of the crest-settlement ratio.

The seismic critical coefficient adopted in the screening level analyses was evaluated through pseudo-static analyses performed with the finite difference method. Critical conditions identified shallow plastic mechanisms activated on the upstream slope.

Earthquake-induced permanent displacements were evaluated using appropriate shape factors, through a series of simplified Newmark-type computations. These involved conventional rigid-block sliding analysis, the Makdisi and Seed procedure modified to better estimate the crest acceleration and some empirical relationships available in the literature.

The screening-level analyses provided scattered results depending on the seismic parameters selected to compute the displacement induced by seismic shaking, with maximum vertical and horizontal crest displacements of 0.20–0.30 m and 0.50–0.73 m, respectively.

As it could be anticipated, much greater displacements were computed using empirical relationships in which the energy content of seismic shaking is accounted for together with its duration, thus identifying the empirical relationships capable to provide a safe estimate of earthquake-induced displacements. Moreover, the analyses pointed out that possible 20% reduction of shear strength results in about 2.5 times larger displacements, again stressing the crucial relevance of a reliable geotechnical characterisation.

For both the ultimate limit states considered in the analyses, and even considering possible reduction of shear strength induced by earthquake loading, all simplified procedures provided crest settlements lower than the available freeboard and crest-settlement ratios lower than those corresponding to the attainment of both a Life and a Collapse Limit State.

All the analyses presented in the paper pointed out the relevant role of earthquake-induced shear strength reduction possibly occurring in the soils of the dam and also highlighted the need of further refinements and higher-level analyses (Cascone et al., 2021) to evaluate the influence of the vertical component of ground motion and of excess pore pressures on the magnitude of earthquake-induced dam displacements.

Authors' statement

The data that has been used is not confidential.

Aknowledgements

The Authors are grateful to the anonymous reviewers for helping to improve the quality of the manuscript. This work is part of the research activities carried out in the framework of the research project of major national interest, PRIN n. 2017YPMBWJ, on "*Risk assessment of Earth Dams and River Embankments to Earthquakes and Floods* (REDREEF)" funded by the Italian Ministry of Education University and Research (MIUR).

Declaration of Competing Interest

None.

References

Aliberti, D., Biondi, G., Cascone, E., Rampello, S., 2019. Performance indexes for seismic analyses of earth dams. In: 7th ICEGE, Rome, Italy, 2019.

Araya, R., Saragoni, R., 1984. Earthquake accelerogram destructiveness potential factor. In: 8th WCEE, San Francisco, 1984, 2, pp. 835–841.

Arias, A., 1970. A measure of earthquake intensity. In: Hansen, R. (Ed.), Seismic Design for Nuclear Power Plants. MIT Press, Cambridge, MA, pp. 438–483.

Bazzurro, P., Cornell, C.A., 1999. Disaggregation of seismic hazard. Bull. Seismol. Soc. Am. 89 (2), 501–520.

Biondi, G., Cascone, E., Rampello, S., 2011. Evaluation of seismic stability of natural slopes. Rivista Italiana di Geotecnica (1), 11–34.

Biondi, G., Cascone, E., Di Filippo, G., 2012. Reliability of empirical relationships for the evaluation of the number of equivalent loading cycles. Rivista Italiana di Geotecnica XLVI (2), 9–39.

Bommer, J.J., Acevedo, A.B., 2004. The use of real earthquake accelerograms as input to dynamic analysis. J. Earthq. Eng. 8 (1), 43–91. Special issue.

Bray, J.D., 2007. Simplified seismic slope displacement procedures. Chapter 14 in. In: Pitilakis, K.D. (Ed.), Earthquake Geotechnical Engineering. Springer, pp. 327–353.

Bray, J.D., Travasarou, T., 2007. Simplified procedure for estimating earthquake-induced deviatoric slope displacements. J. Geotech. Geoenviron. Eng. ASCE 133 (4), 381–392.

Calabresi, G., Rampello, S., Callisto, L., Cascone, E., 2004. Diga S. Pietro sul fiume Osento. Verifica delle condizioni di stabilità e analisi del comportamento in condizioni sismiche. Università di Roma "La Sapienza" Contratto di Ricerca con il Consorzio per la Bonifica della Capitanata (In Italian).

Cascone, E, Biondi, G, Aliberti, D, Rampello, S, 2021. Effect of vertical input motion and excess pore pressures on the seismic performance of a zoned dam. Soil Dynamics and Earthquake Engineering. Submitted for publication.

Catalano, A., Caruana, R., Del Gizzi, F., De Sortis, A., 2013. Observed Behaviour of Italian Dams under Historical Earthquakes. 9th ICOLD European Club Symposium, Venice.

Chen, G., Jin, D., Mao, J., Gao, H., Wang, Z., Jing, L., Li, Y., Li, X., 2014. Seismic damage and behavior analysis of earth dams during the 2008 Wenchuan earthquake, China. Eng. Geol. 180, 99–129.

Crespellani, T., Madiai, C., Vannucchi, G., 1998. Earthquake destructiveness potential factor and slope stability. Geotechnique 48 (3), 411–419.

Eurocode 8-5, 2003. EN 1998-1 (2003). Eurocode 8: Design of Structures for Earthquake Resistance - Part 5: Foundations, retaining structures and Geotechnical Aspects. CEN European Committee for Standardization, Brussels, Belgium.

FEMA, 2005. Federal Guidelines for Dam Safety, Earthquake Analysis and Design of Dams.

Gibbs, H.J., Holtz, W.G., 1957. Research on Determining the Density of Sands by Spoon Penetration Testing, 1. IV ICSMFE, London, pp. 35–39.

Harder, L.F., Bray, J.D., Volpe, R.L., Rodda, K.V., 1998. Performance of earth dams during the Loma Prieta earthquake. Professional paper no.1552-D, The Loma Prieta, California earthquake of October 17, 1989: Performance of the Built Environment. Earth structures and engineering characterization of ground motion. U.S. Geological Survey, Reston Va.

Hsu, C., Vucetic, M., 2006. Threshold shear strain for cyclic pore-water pressure in cohesive soils. J. Geotech. Geoenviron. Eng. ASCE 132 (10), 1325–1335.

Hynes-Griffin, M.E., Franklin, G., 1984. Rationalising the Seismic Coefficient Methods. Miscellaneous Paper GL-84-13, U.S. Army Corps of Engineers, Waterways Experiment Station, Vicksburg, Mississippi, USA.

ICOLD, 2001. Design features of dams to effectively resist seismic ground motion. In: Bulletin 120, Committee on Seismic Aspects of Dam Design. International Commission on Large Dams, Paris, p. 2001.

ICOLD, 2010. Selecting seismic parameters for large dams. In: Guidelines, Revision of Bulletin 72, Committee on Seismic Aspects of Dam Design. International Commission on Large Dams, Paris, p. 2010.

Ishihara, K, 2010. Performance of rockfill dams during recent large earthquakes. In: Prakash, S (Ed.), 5th Int. Conference on Recent Advances in Geotechnical Earthquake Engineering and Soil Dynamics. San Diego, California. University of Missouri-Rolla.

ITASCA, 2011. FLAC – Fast Lagrangian Analysis of Continua – Version 7.0. User's Guide. Itasca Consulting Group, Minneapolis, USA.

JCOLD, 2012. Review of the Cause of Fujinuma-Ike failure - Summary Report - January 25, 2012. http://www.jcold.or.jp/e/activity/FujinumaSummary-rev.120228.pdf.

Jibson, R.W., 1993. Predicting earthquake-induced landslide displacements using Newmark's sliding block analysis. Transp. Res. Rec. 1411.

Joyner, W.B., Boore, D.M., 1981. Peak horizontal acceleration and velocity from strong motion records including records from the 1979 Imperial Valley, California, earthquake. Bull. Seismol. Soc. Am. 71, 2011–2038.

Kulhawy, F.H., Mayne, P.W., 1990. Estimating soil properties for foundation design. In: EPRI Report EL- 6800. Palo Alto, Electric Power Research Institute, p. 306.

Lanzo, G., Pagliaroli, A., Scasserra, G., 2015. Effects of ground motion characteristics on seismic response of earth dams: some remarks on duration parameters and vertical shaking. In: SECED 2015 Conference: Earthquake Risk and Engineering towards a Resilient World 9–10 July 2015, Cambridge, UK.

Locati, M., Camassi, R., Rovida, A., Ercolani, E., Bernardini, F., Castelli, V., Caracciolo, C. H., Tertulliani, A., Rossi, A., Azzaro, R., D'Amico, S., Conte, S., Rocchetti, E., 2016. DBMI15, the 2015 Version of the Italian Macroseismic Database (Istituto Nazionale di Geofisica e Vulcanologia).

Luzi, L, Pacor, F, Puglia, R, 2016. Italian Accelerometric Archive v 2.1. Istituto Nazionale di Geofisica e Vulcanologia, Dipartimento della Protezione Civile Nazionale. https://doi.org/10.13127/ITACA/2.1.

Madiai, C., 2009. Correlazioni tra parametri del moto sismico e spostamenti attesi del blocco di Newmark. In: Rivista Italiana di Geotecnica, pp. 23–43 n.1. (in Italian).

Makdisi, F., Seed, H.B., 1978. Simplified procedure for estimating dam and embankment earthquake induced deformations. J. Geotech. Eng. 104 (7), 849–867.

Masini, L., Callisto, L., Rampello, S., 2015. An interpretation of the seismic behaviour of reinforced-earth retaining structures. Géotechnique 65.5 (2015), 349–358.

Meehan, C.L., Vahedifard, F., 2013. Evaluation of simplified methods for predicting earthquake-induced slope displacements in earth dams and embankments. Eng. Geol. 152, 180–193.

NTC18, 2018. Norme Tecniche per le Costruzioni. Decreto del Ministero delle Infrastrutture e dei Trasporti, January 17, 2018. G.U. n. 42, February 20, 2018 (in Italian).

NTD14, 2014. Norme Tecniche per la progettazione e la costruzione degli sbarramenti di ritenuta (dighe e traverse). June 26, 2014. G.U. n.156, July 8, 2014 (in Italian).

Pagano, L., Sica, S., 2013. Earthquake early warning for earth dams: Concepts and objectives. Nat. Hazards 66 (2), 303–318.

Pagliaroli, A., Lanzo, G., 2008. Selection of real accelerograms for the seismic response analysis of the historical town of Nicastro (Southern Italy) during the March 1638 Calabria earthquake. Eng. Struct. 30, 2211–2222.

Papadimitriou, A., 2019. An engineering perspective on topography and valley effects on seismic ground motion. In: Theme Lecture 7th ICEGE, Rome, Italy, p. 2019.

Papadimitriou, A.G., Bouckovalas, G.D., Andrianopoulos, K.I., 2014. Methodology for estimating seismic coefficients for performance-based design of earth dams and tall embankments. Soil Dyn. Earthq. Eng. 56 (14), 57–73.

PEER, 2016. PEER NGA Ground Motion Database, Pacific Earthquake Engineering Research Center. http://peer.berkeley.edu/nga.

Poulos, H.G., Booker, J.R., Ring, G.J., 1972. Simplified calculation of embankment deformations. Soils Found. 1972 12 (4), 1–17.

Rampello, S., Callisto, L., Fargnoli, P., 2010. Evaluation of slope performance under earthquake loading conditions. Rivista Italiana di Geotecnica 44 (4), 29–41.

Rathje, E.M., Antonakos, G., 2011. A unified model for predicting earthquake-induced sliding displacements of rigid and flexible slopes. Eng. Geol. 122 (1–2), 51–60.

Rathje, E.M., Abrahamson, N.A., Bray, J.D., 1998. Simplified frequency content estimates of earthquake ground motions. J. Geotech. Eng. ASCE 124 (2), 150–159.

Rizzitano, S., Cascone, E., Biondi, G., 2014. Coupling of topographic and stratigraphic effects on seismic response of slopes through 2D linear and equivalent linear analyses. Soil Dyn. Earthq. Eng. 67, 66–84.

Russo, A.D., Sica, S., Del Gaudio, S., De Matteis, R., Zollo, A., 2017. Near-source effects on the ground motion occurred at the Conza Dam site (Italy) during the 1980 Irpinia earthquake. Bull. Earthq. Eng. 15 (10), 4009–4037.

Saygili, G., Rathje, E.M., 2008. Empirical predictive models for earthquake-induced sliding displacements of slopes. J. Geotech. Geoenviron. Eng. ASCE 134 (6), 790–803.

Seed, H.B., 1979. Considerations in the earthquake-resistant design of earth and rockfill dams. Geotechnique 29 (3), 215–263.

Seed, H.B., Idriss, I.M., Lee, K.L., Makdisi, F.I., 1975. Dynamic Analysis of the Slide in the Lower San Fernando Dam during the Earthquake of February 9, 1971. J. Geotech. Eng. Div., ASCE 101 (GT9), 889–911.

Skempton, A.W., 1986. Standard penetration tests procedure and the effects in sands of overburden pressure, relative density, particle size, ageing and overconsolidation. Geotechnique 36 (3), 425–447.

Stucchi, M., Meletti, C., Montaldo, V., Crowley, H., Calvi, G.M., Boschi, E., 2011. Seismic hazard assessment (2003–2009) for the Italian building code. Bull. Seismol. Soc. Am. 101, 1885–1911.

Swaisgood, J, 2003. Embankment dam deformations caused by earthquakes. Proceedings of the 2003 Pacific Conference on Earthquake Engineering, Christchurch, New Zealand. New Zealand Society for Earthquake Engineering Inc.

Trifunac, M.D., Brady, A.G., 1975. A study of the duration of strong earthquake ground motion. Bull. Seismol. Soc. Am. 65, 581–626.

Tropeano, G., Silvestri, F., Ausilio, E., 2017. An uncoupled procedure for performance assessment of slopes in seismic conditions. Bull. Earthq. Eng. 15 (9), 3611–3637.

Vecchietti, A., Cecconi, M., Russo, G., Pane, V., 2019. Seismic vulnerability of a rockfill dam through different displacement-based approaches. J. Earthq. Eng. 1–27.

Vucetic, M., Dobry, R., 1991. Effect of soil plasticity on cyclic response. J. Geotech. Eng. ASCE 117 (1), 89–107.

Wieland, M., 2003. Seismic aspects of dams, General Report Question 83: Seismic Aspects of Dams. International Commission on Large Dams. 21st Congress of ICOLD, Montreal, Canada. June 16-20, 2003.

Wieland, M., 2012. Seismic Design and Performance Criteria for large Storage Dams. 15th WCEE, Lisbon, Portugal, Sep. 24-28, 2012.

Wieland, M., Chen, H., 2009. Lessons learnt from the Wenchuan earthquake. Int. J. Water Power Dam Construct. 36–40. September 2009.

Yegian, M.K., Marciano, E.A., Ghahraman, V.G., 1991. Earthquake-induced permanent deformations: probabilistic approach. J. Geotech. Eng. ASCE CXVII (1), 35–50.